

# Assessment of MERRA-2 Land Surface Energy Flux Estimates

Clara S. Draper \*

*USRA/GESTAR and NASA Global Modeling and Assimilation Office, Greenbelt, MD, USA.*

*Now at CIRES NOAA/ESRL, Physical Sciences Division, Boulder, CO.*

Rolf H. Reichle

*NASA Global Modeling and Assimilation Office, Greenbelt, MD, USA.*

Randal D. Koster

*NASA Global Modeling and Assimilation Office, Greenbelt, MD, USA.*

\* *Corresponding author address:* Clara Draper, NOAA ESRL, Physical Sciences Division, 325

Broadway, Boulder, CO, USA.

E-mail: clara.draper@noaa.gov

## ABSTRACT

12 In the Modern-Era Retrospective analysis for Research and Applications,  
 13 version 2 (MERRA-2) system the land is forced by replacing the model-  
 14 generated precipitation with observed precipitation before it reaches the sur-  
 15 face. This approach is motivated by the expectation that the resultant improve-  
 16 ments in soil moisture will lead to improved land surface latent heating (LH).  
 17 Here we assess aspects of the MERRA-2 land surface energy budget and 2 m  
 18 air temperatures ( $T^{2m}$ ). For global land annual averages, MERRA-2 appears  
 19 to overestimate the LH (by  $5 \text{ W m}^{-2}$ ), the sensible heating (by  $6 \text{ W m}^{-2}$ ),  
 20 and the downwelling shortwave radiation (by  $14 \text{ W m}^{-2}$ ), while underestimat-  
 21 ing the downwelling and upwelling (absolute) longwave radiation (by 10-15  
 22  $\text{W m}^{-2}$  each). These results differ only slightly from those for NASA's previ-  
 23 ous reanalysis, MERRA. Comparison to various gridded reference data sets  
 24 over Boreal summer (June-July-August) suggests that MERRA-2 has particu-  
 25 larly large positive biases ( $>20 \text{ W m}^{-2}$ ) where LH is energy-limited, and that  
 26 these biases are associated with evaporative fraction biases rather than radi-  
 27 ation biases. For time series of monthly means during Boreal summer, the  
 28 globally averaged anomaly correlations ( $R_{anom}$ ) with reference data were im-  
 29 proved from MERRA to MERRA-2, for LH (from 0.39 to 0.48 vs. GLEAM  
 30 data) and the daily maximum  $T^{2m}$  (from 0.69 to 0.75 vs. CRU data). In re-  
 31 gions where  $T^{2m}$  is particularly sensitive to the precipitation corrections (in-  
 32 cluding the central US, the Sahel, and parts of south Asia), the changes in  
 33 the  $T^{2m} R_{anom}$  are relatively large, suggesting that the observed precipitation  
 34 influenced the  $T^{2m}$  performance.

## 35 1. Introduction

36 The NASA Global Modeling and Assimilation Office recently released the Modern-Era Ret-  
37 rospective analysis for Research and Applications, version 2 (MERRA-2; Gelaro and Coauthors  
38 (2017)). This new global reanalysis product replaces and extends the original MERRA atmo-  
39 spheric reanalysis (Rienecker et al. 2011), as well as the MERRA-Land reanalysis (Reichle et al.  
40 2011). In addition to several other major advances, MERRA-2 uses observed precipitation in place  
41 of model-generated precipitation at the land surface during the atmospheric model integration. The  
42 use of observed precipitation in MERRA-2 was refined from the approach used for MERRA-Land  
43 (Reichle et al. 2017b), which was an offline (land only) replay of MERRA forced by atmospheric  
44 fields from MERRA but with the precipitation forcing corrected using gauge-based observations.

45 The motivation for using observed precipitation in reanalyses is that precipitation is the main  
46 driver of soil moisture, which in turn controls the partitioning of incident surface radiation between  
47 latent heat (LH) and sensible heat (SH) fluxes back to the atmosphere. Reichle et al. (2017a)  
48 show that both MERRA-2 and MERRA-Land have improved upon the land surface hydrology of  
49 MERRA, showing better agreement with independent observational time series of soil moisture,  
50 terrestrial water storage, stream flow, and snow amount. Here, we extend this work, by evaluating  
51 the MERRA-2 surface energy budget and 2 m temperatures ( $T^{2m}$ ) over land. In particular, we  
52 focus on whether the improved hydrology in both the (offline) MERRA-Land and the (coupled  
53 land/atmosphere) MERRA-2 data sets translates into the expected improvements to the monthly  
54 mean LH and SH. We also expand previous work by evaluating the reanalyses land surface output  
55 globally, rather than focusing on locations with high quality ground-based observations.

56 We start by comparing the long-term annual global energy budget over land from MERRA-2,  
57 MERRA-Land, and MERRA to state of the art estimates from the literature. These literature

estimates, from Trenberth et al. (2009), Wild et al. (2015), and the NASA Energy and Water Cycle Studies program (NEWS, NSIT (2007); L’Ecuyer et al. (2015)) were each produced by carefully combining multiple input data sets with global energy balance constraints. Taken together they represent our best understanding of the long-term annual mean energy budget over land.

Next, we consider global maps of the performance of the land surface turbulent heat fluxes from each reanalyses, as a step towards linking differences in performance to the dominant local physical processes and to the potential improvements obtained from the use of the observed precipitation in MERRA-2. We focus on the Boreal summer (June-July-August; JJA), since land/atmosphere coupling is strongest and surface turbulent heat fluxes are most active in the summer.

Unfortunately, there are no standard global gridded reference data sets against which the reanalysis LH and SH can be evaluated. Several recent efforts have compared global LH estimates from different combinations of reanalyses, offline land surface models, and diagnostic methods. Most estimates generally agree on the regional patterns and local seasonal cycle of LH, although there is considerable disagreement in the absolute values and temporal behavior across different flux estimates (Jiménez et al. 2011; Mueller et al. 2011; Miralles et al. 2011). Additionally, uncertainty in the basic model structure is the largest source of disagreement (Schlosser and Gao 2010; Mueller et al. 2013). While ground-based observations are available from tower-mounted eddy covariance sensors (e.g., Baldocchi and Coauthors (2001)), the number of towers (in the 100’s) is well below the sampling needed for global estimation (and their locations are not designed to sample globally-representative land cover types). Additionally, the measurements themselves have considerable uncertainty and limited spatial representativeness (up to 1 km).

In the absence of a standard reference, we compare the JJA reanalysis turbulent heat flux estimates to two different gridded reference data sets: Global Land surface Evaporation: the Amsterdam Methodology (GLEAM) (Miralles et al. 2011; Martens et al. 2017) for LH, and Fluxnet-

82 Model Tree Ensembles (MTE) (Jung et al. 2010) for LH and SH. These data sets were selected for  
83 several reasons: i) they are amongst the state of the art, ii) they are available globally for multi-  
84 decadal time periods, iii) they are independent of each other, and iv) they rely on very different  
85 estimation methodologies (water balance modeling for GLEAM, and upscaling of tower measure-  
86 ments for MTE). Since neither GLEAM nor MTE represents direct observations of the turbulent  
87 heat fluxes, we also compare each reanalysis to tower-based eddy covariance observations from  
88 the Fluxnet-2015 data set (Fluxnet 2015). To determine the potential contribution of radiation bi-  
89 ases to regional LH and SH biases, we also compare the reanalyses surface radiation fields for JJA  
90 against gridded observations from the Clouds and the Earth’s Radiant Energy System (CERES)  
91 and Energy Balanced and Filled (EBAF) data set (Kato et al. 2013).

92 Finally, to test whether the changes in the surface energy budget from MERRA to MERRA-  
93 2 have affected the atmospheric boundary layer, we also evaluate the JJA monthly mean daily  
94 minimum and maximum  $T^{2m}$  against observations from the Climatic Research Unit (CRU) at the  
95 University of East Anglia (Harris et al. 2014). Improvements in MERRA-2 due to the use of  
96 observed precipitation cannot be isolated from the many other advances distinguishing MERRA-  
97 2 from MERRA. Consequently, we establish whether the improvements in the surface turbulent  
98 fluxes and  $T^{2m}$  are at least consistent with the expected improvements from the use of observed  
99 precipitation, by cross-referencing the evaluation results against the regional sensitivity to precip-  
100 itation and/or soil moisture.

101 This paper is organized as follows. Section 2 summarizes the reanalysis and reference data sets  
102 used, and Section 3 presents the results, including evaluation of the i) reanalyses annual global  
103 land energy budget averages, ii) the spatially distributed mean JJA energy budget and  $T^{2m}$ , and ii)  
104 the temporal behavior of the JJA turbulent heat fluxes and  $T^{2m}$ . We also identify regions of sensi-

105 tivity to the observed precipitation forcing in MERRA-2, for cross-reference against the evaluation  
106 results. Our findings are summarized in Section 4.

## 107 **2. Methodology and data**

### 108 *a. The reanalyses*

109 The coverage and resolution of each reanalysis is summarized in Table 1, with further details  
110 below. MERRA (Rienecker et al. 2011) and MERRA-2 (Gelaro and Coauthors 2017) are atmo-  
111 spheric reanalyses produced with the NASA Goddard Earth Observing System Version 5 (GEOS-  
112 5) modeling and data assimilation system, and were designed to provide historical analyses of the  
113 hydrological cycle across a broad range of climate time scales. To address shortcomings in the  
114 MERRA land surface hydrology, MERRA-Land (Reichle et al. 2011) was released as an offline  
115 (land only) replay of MERRA, with the model-generated precipitation corrected using rain-gauge  
116 observations and with minor, but important, model parameter changes. MERRA-2 features sev-  
117 eral major advances from MERRA, including an updated atmospheric general circulation model,  
118 an updated atmospheric assimilation system, an interactive aerosol scheme, and the use of ob-  
119 served precipitation at the land surface (and to compute wet aerosol deposition). In addition to  
120 the land model updates from MERRA-Land, MERRA-2 includes several more updates relevant to  
121 the land, as outlined in Reichle et al. (2017a). Most notably, the surface turbulence scheme was  
122 revised, generally resulting in enhanced SH over land (Molod et al. 2015).

123 The method used to apply the observed precipitation at the land surface in MERRA-2 was refined  
124 from that used in MERRA-Land (Reichle and Liu 2014; Reichle et al. 2017b). In MERRA-Land  
125 the precipitation was corrected with daily Climate Prediction Center (CPC) Unified (CPCU; Chen  
126 et al. (2008)) precipitation observations everywhere. For MERRA-2 the input precipitation differs

in two ways: i) in the high latitudes the MERRA-2 model-generated precipitation is retained, and  
ii) over Africa the MERRA-2 precipitation is corrected with pentad-scale blended satellite and  
gauge-based observations from the CPC Merged Analysis of Precipitation (CMAP; Xie and Arkin  
(1997)) and the Global Precipitation Climatology Project (GPCP; Huffman et al. (2009)) version  
2.1.

The land surface turbulent fluxes from the NASA reanalyses (MERRA-2, MERRA-Land, and  
MERRA) have not been explicitly evaluated globally. However, Jiménez et al. (2011) and Mueller  
et al. (2011) both included MERRA LH when merging multiple LH global land data sets into a  
single enhanced estimate (see Section 2.b), and in both studies MERRA was amongst the high-  
est of the input LH estimates used. Additionally, Jiménez et al. (2011) noted a sharp gradient  
in the MERRA LH around 10°S in the tropics that was not present in other LH estimates. This  
bias gradient was traced to MERRA's excessive rainfall canopy interception and precipitation er-  
rors (Reichle et al. 2011). Consequently, the interception reservoir parameters were revised for  
MERRA-Land (and MERRA-2) to eliminate this feature (the interception reservoir update was  
the most significant modeling change from MERRA to MERRA-Land).

An additional reanalysis, ERA-Interim, from the European Centre for Medium Range Weather  
Forecasting (Dee et al. 2011), is included in the evaluation of the temporal behavior of the turbulent  
fluxes. In contrast to the NASA reanalyses, ERA-Interim includes a land surface updating scheme  
(de Rosnay et al. 2014). Specifically, the soil moisture, soil temperature, and snow temperatures  
are updated to minimize errors in the forecast screen-level relative humidity and temperature,  
while the snow depths are updated using satellite- and ground-based snow cover and snow depth  
observations.



149 *b. Annual global land energy budget estimates*

150 We compare the reanalyses annual global land energy budgets to three state of the art estimates,  
151 from Trenberth et al. (2009), Wild et al. (2015), and the NEWS program estimates of L’Ecuyer  
152 et al. (2015). Each of these is based on a weighted merger of multiple modeled and observed data  
153 sets, and each applies to the energy budget at the start of the 21st Century. For Trenberth et al.  
154 (2009) we have used their estimates for the ‘CERES period’ of 2000-2004; Wild et al. (2015)  
155 nominally refers to the same period; while L’Ecuyer et al. (2015) nominally refers to 2000-2009.  
156 Note that the MERRA LH and SH over land were used as one of the inputs in NEWS.

157 These three global energy budget studies all provide continental and oceanic energy estimates,  
158 where ‘continental’ is defined as non-ocean, and so includes land, land-ice, and lakes, but excludes  
159 inland seas. By contrast, the land estimates from MERRA-2, MERRA-Land, and MERRA apply  
160 to the area modeled by the land surface model, excluding land-ice, lakes, and inland seas. The  
161 discrepancy due to the inclusion or exclusion of land-ice is significant: land-ice accounts for 10%  
162 of the continental area, with Antarctica making up 95% of this. NEWS provides energy bud-  
163 gets for each continent separately (L’Ecuyer et al. 2015), and we use their (balance-constrained)  
164 energy budget estimates to approximate the land-only energy budget terms by subtracting the area-  
165 weighted Antarctica estimates from the global continental estimates. We then use our land-only  
166 NEWS estimates to approximate the continental to land ratio for each NEWS energy budget term.  
167 By assuming that the same ratios apply to Trenberth et al. (2009) and Wild et al. (2015) we then  
168 approximate land-only estimates for the latter two studies. L’Ecuyer et al. (2015) and Wild et al.  
169 (2015) both provide uncertainty ranges for their globally averaged continental estimates, which  
170 we have applied unchanged to our approximated land-only estimates.

For LH, we have also used three additional global land annual average estimates from the hydrology community, from Jiménez et al. (2011), Mueller et al. (2011), and Mueller et al. (2013). These estimates are also based on merging modeled and observed estimates. Jiménez et al. (2011) applies to global land (using a similar land definition to the NASA reanalyses) for 1994, while Mueller et al. (2011) applies to the global land area, excluding the Sahara, from 1989-1995, and Mueller et al. (2013) applies to the global land plus Greenland for 1989-2005. As previously noted, MERRA LH was one of the inputs used in the multi-product mergers of Jiménez et al. (2011) and Mueller et al. (2011).

### *c. Gridded reference data sets*

The coverage and resolution of each gridded reference data set, together with a brief summary of important interdependencies with other data sets or reanalyses used in the study and uncertainty estimates (where available) are summarized in Table 2, with further details provided below.

#### 1) GLEAM

GLEAM (version 3.1a) provides daily estimates of terrestrial evapotranspiration, estimated from satellite and reanalysis forcing using a Priestley and Taylor-based model (Miralles et al. 2011; Martens et al. 2017). The precipitation is from the Multi-Source Weighted-Ensemble Precipitation, which is a multi-model merger of established precipitation data sets, including the same CPCU data set used in MERRA-Land and MERRA-2, as well as ERA-Interim precipitation (the latter is used predominantly in the high latitudes, where observed precipitation data sets are more uncertain (Beck et al. 2017)). The net surface radiation and  $T^{2m}$  are from ERA-Interim. Compared to independent observations from 91 flux towers, GLEAM has an average unbiased root mean square

error (ubRMSE; or error standard deviation) of  $20 \text{ Wm}^{-2}$  and an average anomaly correlation of 0.42 (Martens et al. 2017).

## 2) MTE

MTE provides global estimates of carbon dioxide, energy, and water fluxes at the land surface, calculated using a machine learning technique to upscale half-hourly energy balance-corrected eddy covariance observations from 253 Fluxnet tower observations (Jung et al. 2011). The input Fluxnet observations are from the La Thuile data release, an earlier generation of the Fluxnet-2015 data set used here (to be introduced in Section 2.d). CPCU precipitation (again, used directly in MERRA-Land and MERRA-2) and a  $T^{2m}$  data set based on CRU data (Jung et al. 2011) are used as predictive (regression) variables in the MTE. However, this meteorological data has little impact on the MTE monthly anomalies, which are instead driven by the vegetation variability as observed by the fraction of absorbed Photosynthetically Active Radiation (fPAR; Jung et al. (2010)). When 20% of the Fluxnet training data was withheld from the algorithm, the average Root Mean Square Error (RMSE) with the withheld data was  $15 \text{ Wm}^{-2}$ , for both LH and SH, and the average anomaly correlation was 0.57 for LH and 0.60 for SH (Jung et al. 2011). In general, the MTE method is better suited to estimating spatial variability and the seasonal cycle than it is to capturing interannual anomaly patterns (Jung et al. 2009).

## 3) CRU TEMPERATURE DATA

CRU TSv4.00 provides gridded monthly means of the daily mean, minimum, and maximum temperature over land (Harris et al. 2014; University of East Anglia Climate Research Unit et al. 2014). The temperatures are calculated from quality controlled climate station data, which are interpolated onto the grid according to an assumed correlation decay distance (set to 1200 km for

temperature variables). In instances where no station data are available within the assumed decay distance, the published data value defaults to the climatology. Here, such climatological values have been screened out. Also, we require at least 10 data points to estimate each statistic for a given grid cell. Even with this screening, the gridded output will be much less certain when/where station coverage is less dense, which occurs over Africa, South America, central Australia, and the high latitudes.

#### 4) CERES-EBAF RADIATION DATA

CERES-EBAF version 4.00 surface radiances are produced with a radiative transfer model after adjusting modeled and observed input data for consistency with Top of Atmosphere (TOA) CERES-EBAF radiation (Kato et al. 2013). The input data (surface, cloud, and atmospheric properties) are adjusted according to their observation-based estimated uncertainties. The input temperature and humidity profiles and land surface skin temperature ( $T_{skin}$ ) are from NASA's GEOS-5.4.1 modeling and assimilation system, the same system (although a different version) used in MERRA and MERRA-2.

The CERES output shortwave irradiances are primarily determined by (observation-based) TOA radiation and clouds, hence they are reasonably independent of the MERRA and MERRA-2 re-analyses (Kato et al. 2013). On the other hand, the CERES output longwave irradiances, and particularly the upwelling longwave ( $LW_u$ ), are strongly dependent on the GEOS-5  $T_{skin}$  input. However, the CERES algorithm does adjust its input GEOS-5  $T_{skin}$  with observation-based cloud information, so comparison between the CERES-EBAF and GEOS-5  $LW_u$  partly reflects these observation-based adjustments, even though the two fields are not independent. Compared to independent ground-based observations from 24 sites over land, the RMSE of the CERES-EBAF radiation is  $12 \text{ Wm}^{-2}$  for downwelling shortwave ( $SW_d$ ), and  $10 \text{ Wm}^{-2}$  for downwelling long-

237 wave ( $LW_d$ ) (CERES-EBAF 2017). For the regional estimates over land, CERES-EBAF (2017)  
238 estimated the uncertainty to be  $12 \text{ Wm}^{-2}$  for  $SW_d$ ,  $4 \text{ Wm}^{-2}$  for upwelling shortwave ( $SW_u$ ),  $10$   
239  $\text{Wm}^{-2}$  for  $LW_d$ , and  $18 \text{ Wm}^{-2}$  for  $LW_u$ .

## 240 5) GRIDDED DATA SET PROCESSING

241 As noted in Tables 1 and 2 some of the reference data sets and reanalyses used here publish  
242 output that applies only to the land fraction within each grid cell, while others publish a single  
243 estimate that applies to all surface types (land, permanent land-ice, lakes, ocean) within each grid  
244 cell. All of the gridded data sets and reanalyses were screened by removing all grid cells where  
245 the MERRA-2 land fraction was less than 50% (after interpolation to the relevant resolution), and  
246 then aggregated up to monthly means and  $1^\circ$  spatial resolution. All maps of global statistics are  
247 based on the Boreal summer months of JJA only, and each comparison is made over the maximum  
248 available co-incident time period, with the time periods noted in the relevant figure captions. The  
249 anomaly correlations ( $R_{anom}$ ) are evaluated based on anomalies from the mean seasonal cycle  
250 (calculated by subtracting the time period mean separately for each calendar month). The gridded  
251 reference data sets were also used to estimate the annual global land average values, for which the  
252 (interpolated) MERRA-2 land area in each grid cell was used.

### 253 *d. Fluxnet-2015 tower observations*

254 The Fluxnet-2015 (Fluxnet 2015) sites were selected by downloading all Tier 1 observations at  
255 non-irrigated sites within grid cells classified as land at  $1^\circ$  resolution (as derived above in Section  
256 2.c.5), and for which at least a 10 year data record is available. Eddy covariance sensors underesti-  
257 mate turbulent heat fluxes and do not generally close the energy balance (Wilson et al. 2002), hence  
258 we used the Fluxnet-2015 energy balance closure-corrected LH and SH (see Fluxnet (2015) for

259 details of the correction method). While these corrections are rather uncertain, the corrected LH  
 260 and SH showed better agreement with all of the reanalyses in Table 1 in terms of the means across  
 261 all sites and the correlation of the means between the sites (while having negligible impact on the  
 262 mean time series anomaly correlations). The balance-corrected Fluxnet data were then screened  
 263 to retain only days with less than 10% gap-filled data, and only sites with data for at least 2550  
 264 days ( $\sim 70\%$  of 10 years). The monthly means were then calculated for months with at least 15  
 265 days of observations after the above screening, and the corresponding reanalysis monthly means  
 266 were estimated using the same days. The resulting Fluxnet monthly time series were visually in-  
 267 spected, and obviously unrealistic features were removed. Four sites with unrealistic time series  
 268 were removed. Of the remaining 21 stations, just one was in the Southern Hemisphere. Since our  
 269 evaluation focuses on the Boreal summertime, this site was excluded. The remaining 20 sites that  
 270 have been used in this study are listed in supplemental Table 1.

### 271 **3. Results**

#### 272 *a. Annual global land energy budgets*

273 The globally averaged annual land energy budget estimates for MERRA-2, MERRA-Land, and  
 274 MERRA are illustrated in Figure 1, with numerical values given in Table 3. For each term, the  
 275 estimates for MERRA-2 and MERRA are similar (within  $2\text{--}3\text{ }Wm^{-2}$ ), while the partitioning of  
 276  $R_{net}$  into LH and SH differs for MERRA-Land, which is shifted towards greater SH. Compared to  
 277 MERRA, MERRA-Land has  $11\text{ }Wm^{-2}$  more SH, and  $8\text{ }Wm^{-2}$  less LH, with the difference in  $R_{net}$   
 278 due to decreased  $LW_u$  (recall that in the offline MERRA-Land  $SW_{net}$  and  $LW_d$  are taken directly  
 279 from MERRA).

Figure 1 also includes the energy budget estimates from the literature (see Section 2.b), as well as the annual global land averages for each of the gridded reference data sets in Table 2. In Figure 1a, the MERRA-2 and MERRA global land LH are higher than all of the other estimates (although MERRA-2 is within the Jiménez et al. (2011) and Wild et al. (2015) confidence intervals). The three (land-adjusted) LH estimates from the global energy budget studies (Trenberth et al. (2009), Wild et al. (2015), and NEWS) are very similar to each other, and to MTE, GLEAM, Mueller et al. (2011), and MERRA-Land (all are within  $1 \text{ Wm}^{-2}$ ). While the other two LH estimates from the hydrology community (Jiménez et al. (2011) and Mueller et al. (2013)) are higher, they are not as high as MERRA-2 and MERRA. Compared to the average of the three global land energy budget estimates, the MERRA-2 LH is biased high by  $6 \text{ Wm}^{-2}$  (15%), while MERRA is biased high by  $9 \text{ Wm}^{-2}$  (21%), and MERRA-Land is much closer, being biased high by just  $1 \text{ Wm}^{-2}$  (2%).

For the global land SH in Figure 1b, MERRA-2 and MERRA are both higher than Trenberth et al. (2009) and Wild et al. (2015), although lower than NEWS (but within the NEWS confidence interval) and very close (within  $1 \text{ Wm}^{-2}$ ) to MTE. Compared to the average of the three global land energy budget estimates, MERRA-2 is biased high by  $5 \text{ Wm}^{-2}$  (15%) and MERRA by  $4 \text{ Wm}^{-2}$  (12%), while MERRA-Land is much higher, with a bias of  $15 \text{ Wm}^{-2}$  (42%).

The positive biases in both LH and SH from the reanalyses indicate a positive bias in the incident energy at the land surface. Indeed, Figure 1g shows that the reanalyses  $R_{net}$  exceed the three global energy budget estimates, although MERRA-2 (the lowest of the reanalyses) is only slightly higher ( $2 \text{ Wm}^{-2}$ ) than the CERES-EBAF value. Compared to the average of the three global energy budget estimates, the  $R_{net}$  biases are  $12 \text{ Wm}^{-2}$  (15%) for MERRA-2,  $13 \text{ Wm}^{-2}$  (17%) for MERRA, and  $16 \text{ Wm}^{-2}$  (21%) for MERRA-Land. Figures 1c-f show that the positive  $R_{net}$  bias in MERRA-2 and MERRA is made up of a large positive bias in  $SW_d$  combined with insufficient  $LW_u$ , both partly offset by underestimated  $LW_d$ . For  $SW_d$  (Figure 1c) MERRA-2 and MERRA are higher

304 than all three global land energy budget estimates and CERES-EBAF, with a bias compared to the  
 305 the three-product average of  $14 \text{ Wm}^{-2}$  (7%) for MERRA-2 and  $16 \text{ Wm}^{-2}$  (8%) for MERRA.  
 306 For  $SW_u$  (Figure 1d), MERRA-2 and MERRA are both above NEWS, Trenberth et al. (2009),  
 307 and CERES-EBAF, but below Wild et al. (2015) (although within the confidence interval). Both  
 308 are biased high by  $3 \text{ Wm}^{-2}$  (8%), compared to the three-product average. For  $LW_d$  (Figure 1e),  
 309 MERRA-2 and MERRA are lower than the of the other estimates, with biases of  $-11 \text{ Wm}^{-2}$  (-  
 310 3%) for MERRA-2 and  $-10 \text{ Wm}^{-2}$  (-3%) for MERRA against the three-product average. For  
 311  $LW_u$  (Figure 1f) MERRA-2, MERRA-Land, and MERRA are again lower than the other plotted  
 312 estimates, with biases of  $-11 \text{ Wm}^{-2}$  (-3%) for MERRA-2,  $-13 \text{ Wm}^{-2}$  (-3%) for MERRA-Land,  
 313 and  $-10 \text{ Wm}^{-2}$  (-3%) for MERRA.

314 The literature estimates in Figure 1 are presented as long term means, and each represents dif-  
 315 ferent temporal and spatial coverage. Likewise, the annual global land averages for the gridded  
 316 reference data sets in Figure 1 are based on the full available (spatial and temporal) coverage for  
 317 each. However, the gridded reference data sets and reanalyses can be cross-screened to ensure that  
 318 they are compared with consistent coverage. With this cross-screening, the MERRA-2 LH bias  
 319 estimate is  $7 \text{ Wm}^{-2}$  vs. GLEAM, or  $9 \text{ Wm}^{-2}$  vs. MTE, while the SH bias is  $1 \text{ Wm}^{-2}$  vs. MTE,  
 320 and the radiation biases vs. CERES-EBAF are  $10 \text{ Wm}^{-2}$  for  $SW_u$ ,  $2 \text{ Wm}^{-2}$  for  $SW_d$ ,  $-18 \text{ Wm}^{-2}$  for  
 321  $LW_d$ ,  $-11 \text{ Wm}^{-2}$  for  $LW_u$ , and  $<0.5 \text{ Wm}^{-2}$  for  $R_{net}$ . In general, the above-quoted biases (calculated  
 322 after cross-screening) are all close (within  $1 \text{ Wm}^{-2}$ ) to the values estimated from the data plotted  
 323 in Figure 1 (which does not include cross-screening), with the exception of the LH bias vs. MTE,  
 324 which is  $6 \text{ Wm}^{-2}$  without cross-screening (compared to  $9 \text{ Wm}^{-2}$ ). This discrepancy is due to the  
 325 MTE global mean being lower than it otherwise would be, due to the lack of coverage over the  
 326 Sahara (which has near-zero annual mean LH).



## *b. Land-atmosphere coupling and the MERRA-2 precipitation corrections*

Here, we identify regions where, in MERRA-2, i) LH is sensitive to precipitation (or soil moisture), and ii) the daily maximum  $T^{2m}$  ( $T_{max}^{2m}$ ) is sensitive to the applied precipitation corrections. These regions can then be used to determine where the change in performance from MERRA to MERRA-2 is most likely associated with the precipitation corrections. Note that for part ii) above, the diurnal temperature range could be expected to have a stronger signal of the daytime turbulent heat fluxes (Betts et al. 2017), however a preliminary comparison (not shown) revealed similar results for DTR and  $T_{max}^{2m}$ , and we have presented the results for  $T_{max}^{2m}$  since this variable is included in the published MERRA-2 data sets.

### 1) SOIL MOISTURE AND LATENT HEATING

To first order, LH (or evapotranspiration) from soil and vegetation surfaces can be conceptualized as either a moisture- or energy-limited process. In drier conditions (i.e., for soil moisture below some critical point), LH is moisture-limited in that it is restricted by the amount of soil moisture available for evapotranspiration. Temporal variations in LH will then be correlated with the plant available soil moisture (principally, the soil moisture in the root-zone). In contrast, in more humid conditions LH is energy limited; there is sufficient soil moisture available for evapotranspiration, so LH proceeds at the maximum rate determined by atmospheric water demand, and temporal variations in LH are accordingly correlated with temporal variations in atmospheric demand (net radiation, atmospheric humidity deficit, and wind), rather than soil moisture.

Figure 2 shows the squared correlation between the JJA monthly anomaly MERRA-2 LH and rootzone soil moisture ( $R_{anom}^2(LH, SM)$ ). Lower  $R_{anom}^2(LH, SM)$  indicates a tendency towards energy-limited LH, which for the Boreal summer occurs in the high latitudes, central and eastern Europe, the eastern US, south China, and much of the tropics (the Amazon, equatorial Africa, and

southeast Asia). On the other hand, higher  $R_{anom}^2(LH, SM)$  indicates a tendency towards moisture-limited LH, and occurs across the remainder of the low and mid-latitudes. While we have plotted JJA to focus on the Boreal summer, there are still regions of moisture-limited LH in the southern hemisphere during Austral winter, specifically in arid regions (southern Africa, much of Australia, and the desert and steppe regions of South America).

## 2) PRECIPITATION FEEDBACK ON AIR TEMPERATURE

Figure 3 shows maps of the squared anomaly correlation ( $R_{anom}^2$ ) between anomaly timeseries of JJA MERRA-2 monthly  $T_{max}^{2m}$  and anomaly timeseries of 2-month (current + previous month) averaged MERRA-2 precipitation. For example, the June  $T_{max}^{2m}$  is compared to the (May+June) precipitation, while the July  $T_{max}^{2m}$  is compared to the (June+July) precipitation, and so on. The precipitation is lagged like this to allow the precipitation signal to accumulate in the soil, and influence the subsequent  $T_{max}^{2m}$ . In Figure 3a the MERRA-2 model-generated precipitation (PRECTOT) is used, while in Figure 3b the MERRA-2 observation-corrected precipitation (PRECTOTCORR) is used. The  $R_{anom}^2$  are plotted only for negative  $R$  values, since the dominant local relationship between precipitation and daytime temperature is negative (i.e., under moisture-limited conditions, reduced precipitation leads to reduced soil moisture, which limits LH and increases SH and  $T_{max}^{2m}$ ). Figure 3b reflects the modeled relationship in MERRA-2 between precipitation falling on the surface and  $T_{max}^{2m}$ . Even with the difference in time periods, the patterns are similar to those found across the contiguous U.S. from observations by Koster et al. (2015).

Figure 3c then shows the difference between  $R_{anom}^2(T_{max}^{2m}, PRECTOTCORR)$  and  $R_{anom}^2(T_{max}^{2m}, PRECTOT)$ . This difference ( $\Delta R_{anom}^2$ ) is the increase in the fraction of variance in  $T_{max}^{2m}$  explained by the (observed) precipitation seen by the land (PRECTOTCORR) over that explained by the model-generated precipitation (PRECTOT). It thus provides a measure of

373 the local impact of the observed precipitation on the MERRA-2  $T_{max}^{2m}$ . This measure is sensitive  
374 to both the magnitude of the precipitation corrections and the local response of the atmospheric  
375 model to those corrections. Note that the lack of sensitivity in the high latitudes was inevitable for  
376 this metric, since the model-generated precipitation is used there.

377 For the Boreal summer, the strongest impact of the observed precipitation, which can explain  
378 more than 25% of the  $T_{max}^{2m}$  variance, is indicated in the central US, central America, the northern  
379 tip of South America, across a broad swath along the Sahel, and parts of south Asia. Note that  
380 these regions do not directly correspond to the regions of strongest moisture-limited LH in Figure  
381 2, for at least two reasons. First, a strong sensitivity of evapotranspiration to soil moisture (Figure  
382 2) does not imply that the soil moisture variations are locally strong enough to induce large evap-  
383 otranspiration variations and thus large impacts on air temperature (Figure 3c). Second, as noted  
384 previously, the plotted sensitivity also includes a signal of the size of the precipitation corrections,  
385 and so will be enhanced where the differences between the model-generated and observation-  
386 corrected precipitation are larger.

387 Figure 3c is consistent with previous studies identifying hot-spots of strong coupling between  
388 the land and  $T^{2m}$ . In particular Koster et al. (2006) and Miralles et al. (2012) both identify similar  
389 regions of strong coupling centered on the central US/central America and the Sahel, although  
390 they do not agree as well over south Asia. Over South Asia Koster et al. (2006) does not locate a  
391 hotspot, while Miralles et al. (2012) identifies India as having the strongest coupling, and Figure  
392 3c suggests patchy regions of coverage spanning from southeast Asia through the north of India.

393 For reference, the corresponding maps for the Austral summer (December-January-February)  
394 are shown in supplemental Figure 1 for  $R_{anom}^2(LH, SM)$  and supplemental Figure 2 for the sensi-  
395 tivity to the precipitation corrections. In supplemental Figure 1, the  $R_{anom}^2(LH, SM)$  over Austral  
396 summer again shows the expected pattern of moisture-limited LH in drier areas of the summer

hemisphere (almost everywhere, outside of the tropics). As with the Boreal summer, regions of moisture-limitation LH extend into the winter Hemisphere. However, the effect of reduced radiation close to the poles is now evident in the switch to energy-limited LH, even in arid regions that are poleward of around  $50^\circ$  (such as central Asia). Supplemental Figure 2 shows strong sensitivity of  $T_{max}^{2m}$  to the precipitation corrections across nearly all of the southern Hemisphere, including the Amazon and tropical Africa. Since these latter two areas typically have saturated soils, this strong signal is unlikely due to the precipitation-soil moisture pathway, and is perhaps due to sensitivity of evaporative cooling from the canopy interception to changes in precipitation supply to the interception reservoir.

### c. Biases over Boreal summer

In Section 3.a, the biases in the reanalyses' global land energy budgets were provided as annual means. The seasonal cycle of the monthly mean global land biases (not shown) reveal that the largest global land biases for all budget terms occur in the Boreal summer (JJA). Below, maps of these JJA biases are presented and discussed, together with the corresponding biases in 2 m air temperatures.

#### 1) ENERGY BUDGET TERMS

Figure 4 shows maps of the reanalyses' JJA biases in LH and SH compared to each of GLEAM and MTE. For LH, the regions of positive and negative biases relative to GLEAM or MTE are similar (compare the first and second columns of Figure 4). For both, the LH biases depend on the local LH regime, with energy-limited regions (low  $R_{anom}^2(LH, SM)$  in Figure 2) generally having larger positive LH biases ( $> 20 \text{ W m}^{-2}$ ; e.g., for MERRA-2 in Figures 4d,e across the tropics, south Asia, and the northern high latitudes), while moisture-limited regions (high  $R_{anom}^2(LH, SM)$  in

Figure 2) tend to have smaller biases (magnitude  $< 10 W m^{-2}$ ). Consequently, the spatial correlation between  $R_{anom}^2(LH, SM)$  (as plotted in Figure 2) and the MERRA-2 LH biases is -0.65 for GLEAM and -0.73 for MTE.

The MERRA LH biases (Figures 4j,k) show some of the same features as for MERRA-2, again with a tendency for large positive biases in energy-limited LH regimes. The most prominent difference is the sharp bias gradient in MERRA around  $10^\circ S$  (most notable in South America). As discussed in Section 2.b, this is associated with the unrealistically large rainfall interception reservoir in MERRA, combined with the MERRA precipitation errors; these problems have been alleviated in MERRA-2 (and MERRA-Land). Additionally, there are some isolated regions of large positive biases in moisture-limited regimes in MERRA that are removed in MERRA-2 (and MERRA-Land), such as in Mexico and south India.

Overall, in energy-limited regions ( $R_{anom}^2(LH, SM) < 0.5$  in Figure 2) the area-averaged LH bias in MERRA-2 ( $25.5 W m^{-2}$  compared to GLEAM,  $29.9 W m^{-2}$  compared to MTE) was slightly higher than for MERRA ( $24.1 W m^{-2}$  compared to GLEAM,  $27.6 W m^{-2}$  compared to MTE), both of which are much higher than for MERRA-Land ( $11.3 W m^{-2}$  compared to GLEAM, and  $7.6 W m^{-2}$  compared to MTE). In contrast, in moisture-limited LH regions ( $R_{anom}^2(LH, SM) > 0.5$  in Figure 2), the area-averaged LH bias is highest in MERRA ( $7.0 W m^{-2}$  compared to GLEAM,  $5.2 W m^{-2}$  compared to MTE), and reduced in MERRA-2 ( $3.8 W m^{-2}$  compared to GLEAM,  $1.5 W m^{-2}$  compared to MTE), and even further reduced in MERRA-Land ( $0.3 W m^{-2}$  compared to GLEAM,  $-2.9 W m^{-2}$  compared to MTE).

The third column of Figure 4 shows the reanalyses biases in SH compared to MTE. In general, the SH biases for each reanalyses have an inverse relationship with the LH biases in the first two columns (for MERRA-2, the spatial correlation between the SH biases and the LH biases is -0.68 for GLEAM LH and -0.78 for MTE LH). Consequently, the evaporative fraction

443 (EF=LH/(LH+SH)) biases compared to MTE in the first column of Figure 5 show a spatial pattern  
444 very similar to that of the LH biases (for MERRA-2, the spatial correlation between MTE LH and  
445 EF biases is 0.83).

446 The sum of LH and SH approximates the net incoming radiation (after neglecting the ground heat  
447 flux and temporal change in  $T_{skin}$ ). The second and third columns of Figure 5 show, respectively,  
448 the biases in the reanalyses LH+SH sum compared to MTE and the biases in their  $R_{net}$  compared  
449 to CERES-EBAF. There is a weak agreement between the  $R_{net}$  biases suggested by MTE and  
450 CERES-EBAF (for MERRA-2, the spatial correlation is 0.46). Comparison to MTE (Figures 5,  
451 second column) suggests that the reanalyses net surface radiation tends to be overestimated, with  
452 the largest biases ( $>30 \text{ Wm}^{-2}$ ) occurring over the Amazon, the horn of Arica, and the Tibetan  
453 Plateau. While comparison to CERES-EBAF (Figure 5, third column) also suggests relatively  
454 large positive biases over the Tibetan Plateau and the horn of Africa, these positive biases are  
455 smaller in both magnitude and regional extent than was suggested by MTE. Additionally, CERES-  
456 EBAF also indicates strong negative biases ( $<-30 \text{ Wm}^{-2}$ ) over the Sahel and the southeast US,  
457 particularly in MERRA-Land (Figure 5i) and MERRA (Figure 5l). Finally, inter-comparing the  
458  $R_{net}$  biases for each reanalyses shows qualitatively that the broad patterns are similar in MERRA-2  
459 and MERRA (also MERRA-Land), although MERRA has a tendency towards larger (positive and  
460 negative) biases.

461 There is no obvious correspondence between the regional biases in the LH (compared to  
462 GLEAM or MTE) and the regional biases in  $R_{net}$  (compared to either MTE LH+SH or CERES-  
463 EBAF). For example, the spatial correlations are less than 0.1 between the MERRA-2 LH bias  
464 (implied by comparison to GLEAM or MTE), and the MERRA-2 LH+SH bias (implied by MTE).  
465 Likewise, the spatial correlations are again less than 0.1 between the MERRA-2 LH bias (implied  
466 by GLEAM or MTE) and the MERRA-2  $R_{net}$  bias (implied by CERES-EBAF). This suggests then

467 that the pattern of regional biases in the reanalyses LH for JJA (compared to either GLEAM or  
468 MTE) are associated with differences in the partitioning of incoming radiation into LH and SH,  
469 rather than with differences in the surface radiation (compared to MTE or CERES-EBAF) itself.

470 While radiation biases do not appear to be the main predictor of LH biases, biased radiation will  
471 results in biased LH and/or SH. Hence, we have partitioned the JJA  $R_{net}$  bias between MERRA-2  
472 and CERES-EBAF into the individual contributions from each radiation term. Figure 6 shows the  
473 JJA biases between MERRA-2 and CERES-EBAF for the  $SW_{net}$ ,  $LW_d$ , and  $LW_u$ . In terms of the  
474 direction of the biases, the broad patterns of regional biases in the radiation terms are unchanged  
475 from MERRA (not shown). The direction of the regional  $R_{net}$  biases for MERRA-2 in Figure 5f  
476 largely mirror the regional  $SW_{net}$  biases in Figure 6d (spatial correlation: 0.75), the main exception  
477 being over the southeast US. The LW biases are somewhat balanced, in that both are negative  
478 across most of the domain, with the  $LW_d$  bias in Figure 6e typically being slightly more negative  
479 than the  $LW_u$  bias in Figure 6f. Both have relatively large negative biases (magnitude  $> 30 \text{ Wm}^{-2}$ )  
480 in northern hemisphere desert regions, and smaller (magnitude:  $10\text{-}20 \text{ Wm}^{-2}$ ) negative biases  
481 elsewhere. The spatial distribution of the  $SW_{net}$  biases mirrors that of the downwelling shortwave  
482 ( $SW_d$ , not shown), indicating that the  $SW_{net}$  biases are primarily driven by  $SW_d$  differences rather  
483 than differences in the surface albedo used in CERES-EBAF and GEOS-5. The above patterns  
484 of overestimated  $SW_{net}$  (or  $SW_d$ ) and underestimated  $LW_d$  across much of the globe are consistent  
485 with a known tendency for the GEOS-5 systems to underestimate mid-latitude continental cloud  
486 cover (Molod et al. 2012; Wang and Dickinson 2013; Gelaro and Coauthors 2015).

487 The  $LW_u$  is calculated from the  $T_{skin}$ , and the negative biases in MERRA-2 (and also MERRA  
488 and MERRA-Land) indicate a cool bias in the model  $T_{skin}$ . At 285 K, a  $LW_u$  bias of  $10 \text{ Wm}^{-2}$  is  
489 roughly equivalent to a  $T_{skin}$  bias of 2 K. Recall that the CERES-EBAF  $LW_u$  is not independent of  
490 the MERRA suite of reanalyses, due to its use of GEOS-5  $T_{skin}$ . However, the input GEOS-5  $T_{skin}$

491 is adjusted within the CERES-EBAF algorithm to constrain the TOA irradiance, so comparison  
492 of GEOS-5 and CERES  $LW_u$  indicates the adjustment required to the GEOS-5  $T_{skin}$  to balance the  
493 TOA fluxes. Previous work has also suggested that the GEOS-5  $T_{skin}$  is underestimated, partic-  
494 ularly in dry regions. For example, in agreement with our Figure 6f, Draper et al. (2015) found  
495 large cool biases in the GEOS-5  $T_{skin}$  over desert regions in summer (their Fig. 5), compared to  
496 remotely sensed observations. As argued in Draper et al. (2015), this GEOS-5  $T_{skin}$  cool bias is,  
497 at least in part, caused by the model's  $T_{skin}$  definition differing from that of a true skin layer from  
498 which  $LW_u$  is emitted (or as is observed in the thermal infrared).

499 In summary, the pattern of regional LH biases in the reanalyses suggested by GLEAM and MTE  
500 are very similar. This result adds confidence to the use of GLEAM and MTE for estimating re-  
501 gional biases in the reanalyses. As with the annual global land averages in Figure 1, the maps  
502 presented here suggest that MERRA-2 and MERRA (but not MERRA-Land) have a general ten-  
503 dency to overestimate LH. If the GLEAM, MTE, and CERES-EBAF regional means are assumed  
504 to be more accurate than the reanalyses, the above comparisons suggest that in energy-limited  
505 regions, MERRA-2 (and MERRA) overestimate LH due to an overestimated evaporative fraction  
506 (i.e., too much incoming radiation is converted to LH rather than SH). There is little change in the  
507 global average biases from MERRA to MERRA-2. However, there are some isolated regions in  
508 Mexico and south Asia that are typified by moisture-limited LH, where MERRA has positive LH  
509 biases associated with overestimated EF, while MERRA-2 and MERRA-Land have much smaller  
510 biases. The precipitation corrections in MERRA-2 (and MERRA-Land) removed a relatively large  
511 amount of precipitation across these locations (Reichle et al. (2017b); their Figure 3b), strongly  
512 suggesting that the use of precipitation observations in these products reduced the LH biases.



## 2) AIR TEMPERATURE

The biases in the MERRA-2 and MERRA JJA monthly mean daily minimum, daily maximum, and diurnal range in  $T^{2m}$ , relative to the CRU data set, are shown in Figure 7 ( $T^{2m}$  is not calculated by the land-only MERRA-Land system). For the daily minimum  $T^{2m}$  ( $T_{min}^{2m}$ ) in the left column, both reanalyses tend towards positive (warm) biases, particularly MERRA. For the daily maximum  $T^{2m}$  ( $T_{max}^{2m}$ ) in the center column, MERRA-2 tends towards cool biases, with patches of warm biases across central Asia and the Arabian Peninsula (investigation of the large positive bias in the Arabian Peninsula suggests it is associated with an error in the CRU reference data, rather than the reanalyses). For MERRA, these patches of positive bias are expanded to cover most of the desert region in the northern hemisphere, and also much of the southern hemisphere. For the diurnal temperature range (DTR) in the third column, the MERRA-2 biases inherit the broad spatial pattern of the  $T_{max}^{2m}$  biases, while for MERRA some of the large positive  $T_{max}^{2m}$  biases are offset in the DTR by co-located positive  $T_{min}^{2m}$ .

The LH and SH biases in Figures 4 and the DTR biases in Figure 7 show some of the expected regional similarities. In particular, in the high latitudes and the Amazon MERRA-2 has relatively large positive LH biases (and negative SH biases) and relatively large negative DTR biases. MERRA also has overestimated LH and underestimated DTR in the same regions, as well as in southeast Asia and central America. This is consistent with an underestimated DTR caused by underestimated SH (and overestimated LH), particularly given that the  $R_{net}$  bias is generally neutral in these regions in Figure 5. It should however be noted that the high latitudes and the Amazon regions are both data-scarce, and both the reanalyses and reference data sets are less well constrained. In other regions there is less correspondence. For example the western US also has underestimated DTR for MERRA and MERRA-2, while neither GLEAM nor MTE suggests over-

536 estimated LH. Over all, the spatial correlations between the LH biases and DTR biases are rather  
537 low (for MERRA-2, they are -0.38 for GLEAM and -0.47 for MTE).

538 Recall that in Section 3.c.1 above, the CERES-EBAF comparison suggested that the MERRA-2  
539 (and MERRA)  $T_{skin}$  is generally biased cool, with larger cool biases in desert areas. However, a  
540 comparison of the  $LW_u$  biases in Figure 6f to the  $T_{min}^{2m}$  and  $T_{max}^{2m}$  biases in Figures 7d,e shows little  
541 correspondence between them, and in particular the regions of relatively large cool  $T_{skin}$  biases  
542 (underestimated  $LW_u$ ) in the northern hemisphere deserts do not have cool biases in either  $T_{max}^{2m}$   
543 and  $T_{min}^{2m}$ . This apparent contradiction between the temperature biases suggested by comparison  
544 to the CERES-EBAF  $LW_u$  ( $\sim T_{skin}$ ) and the CRU  $T^{2m}$  does not necessarily imply that one of these  
545 data sets is incorrect, given the likelihood mentioned above that the model  $T_{skin}$  biases are at least  
546 partly associated with the model definition of  $T_{skin}$ .

#### 547 *d. Turbulent heat flux anomaly correlations over Boreal summer*

548 Here the monthly mean turbulent heat flux time series are evaluated over Boreal summer based  
549 on their temporal correlations ( $R_{anom}$ ) with the reference data sets. Figure 8 shows maps of the  
550 JJA  $R_{anom}$  for each of the NASA reanalyses (MERRA-2, MERRA-Land, and MERRA) and ERA-  
551 Interim, with the  $R_{anom}$  calculated separately vs. each of the GLEAM and MTE turbulent heat  
552 fluxes. For LH, the regional patterns in the  $R_{anom}$  vs. either GLEAM (Figure 8, first column) or  
553 MTE (Figure 8, second column) show some similar features (for MERRA-2, spatial correlation  
554 between Figures 8a and 8b: 0.69). Comparison to Figure 2 again suggests some dependence on  
555 the LH regime. In the Northern Hemisphere, the LH  $R_{anom}$  is generally highest ( $\sim 0.6$ ) in regions  
556 where LH is moisture-limited, and generally much lower ( $<0.2$ ) where LH is energy-limited. The  
557 two exceptions are the high latitudes, which have high LH  $R_{anom}$  and energy-limited LH, and the

558 Sahara, which has low LH  $R_{anom}$  and is moisture-limited (although LH variability in the Sahara is  
559 very low, making the signal susceptible to noise).

560 The  $R_{anom}$  patterns for ERA-Interim in the final row of Figure 8 provide some additional context  
561 for evaluating the NASA reanalyses. The LH  $R_{anom}$  values are generally higher for ERA-Interim  
562 than for the NASA reanalyses. As for MERRA-2, the ERA-Interim  $R_{anom}$  vs MTE is relatively  
563 low in many energy-limited LH regimes (including the eastern US, tropics, and south Asia), while  
564 the  $R_{anom}$  for ERA-Interim vs. GLEAM is more spatially consistent, in contrast to the  $R_{anom}$  for  
565 MERRA-2. The relatively high  $R_{anom}$  between GLEAM and ERA-Interim LH in energy-limited  
566 LH regimes may well be due to GLEAM having used ERA-Interim radiation and temperature,  
567 since it is in these regions that these fields will have the strongest influence on the LH. On the  
568 other hand, the lower  $R_{anom}$  between the NASA reanalyses and the LH reference data sets (and  
569 also between ERA-Interim and MTE) could be attributed to errors in both the reference data sets  
570 and the reanalyses under energy-limited conditions. For MTE, this result was expected because  
571 MTE is thought to be more reliable in estimating temporal variability in moisture limited areas,  
572 since its temporal variability is largely driven by fPAR (Jung et al. 2010).

573 Moving on to SH, the third column of Figure 8 shows the  $R_{anom}$  vs. MTE for each reanalysis.  
574 The regional patterns are similar to those for LH, with higher  $R_{anom}$  ( $>0.5$ ) in moisture-limited  
575 LH regions, and lower ( $< 0.2$ ) values elsewhere. ERA-Interim  $R_{anom}$  vs. MTE is generally higher  
576 than the NASA reanalyses, with values greater than 0.5 across most of the globe (and particularly  
577 in the Northern Hemisphere). Despite the improved LH from MERRA-Land, the SH  $R_{anom}$  vs.  
578 MTE is lower than for MERRA (or MERRA-2).

579 Globally averaged, the rank order of the mean LH  $R_{anom}$ , while rather low, is the same vs. ei-  
580 ther GLEAM or MTE and follows the expected progression of improvement from MERRA, to  
581 MERRA-Land, and then to MERRA-2. GLEAM suggests a larger improvement, from a globally

582 averaged  $R_{anom}$  of 0.39 for MERRA to 0.48 for MERRA-2, with MERRA-Land falling in be-  
 583 tween (0.45). MTE suggests an improvement from 0.29 for MERRA to 0.34 for MERRA-2, with  
 584 MERRA-Land again falling in between (0.32). For SH, the globally averaged  $R_{anom}$  vs. MTE is  
 585 similar for MERRA (0.36) and MERRA-2 (0.37), but is much lower for MERRA-Land (0.28). For  
 586 ERA-Interim, the global mean  $R_{anom}$  for LH is  $\sim 0.1$  higher than for MERRA-2 (0.60 vs. GLEAM,  
 587 and 0.44 vs. MTE) and  $\sim 0.2$  higher for SH (0.46 vs. MTE). The better agreement between ERA-  
 588 Interim and the reference data sets could be a consequence of the land surface updates applied in  
 589 ERA-Interim, which indirectly targets the turbulent heat fluxes. (Although recall that the relatively  
 590 strong agreement between the GLEAM and ERA-Interim LH will partly reflect their dependence;  
 591 see Section 2.c.2).

#### 592 *e. Comparison to Fluxnet tower data*

593 Since the reference data sets used above do not represent direct observations, we now com-  
 594 pare the globally-averaged LH and SH statistics from Section 3.a (for the annual mean turbulent  
 595 heat fluxes over land), and Section 3.d (for the mean JJA  $R_{anom}$ ) to statistics calculated against  
 596 Fluxnet-2015 tower observations. Figure 9 shows the annual mean of the turbulent fluxes aver-  
 597 aged across the 20 tower sites for the Fluxnet (eddy-covariance) measurements themselves and for  
 598 each reanalysis and reference data set averaged across the 20 Fluxnet locations, with the global  
 599 land annual means (from Figure 1) included for reference. For LH, comparison to the Fluxnet  
 600 observations agrees with the results from the global land comparison in Section 3.a, again sug-  
 601 gesting that the MERRA-2 LH is biased high, although the Fluxnet observations suggest a larger  
 602 bias (of  $12 \text{ Wm}^{-2}$ , or 30%) than was suggested by the global comparison (estimated as  $6 \text{ Wm}^{-2}$   
 603 in Section 3.a). Averaged across the 20 Fluxnet sites, the MTE LH is very close to the Fluxnet  
 604 data (within  $0.5 \text{ Wm}^{-2}$ ), while GLEAM is slightly higher. For the interested reader, supplemental

605 Figure 3 shows scatterplots comparing the MERRA-2 and reference data set LH annual means at  
606 the 20 individual sites.

607 For SH, the Fluxnet observations agree less well with the global land comparison. First, the  
608 annual mean of the Fluxnet data is about  $10 \text{ Wm}^{-2}$  below the global mean estimates from the  
609 other reference data sets. For each of the global reference data sets and reanalyses, the annual  
610 average over the 20 Fluxnet sites is also  $15\text{-}20 \text{ Wm}^{-2}$  lower than the global average, suggesting  
611 that the relatively low Fluxnet annual mean is associated with the spatial sampling of the Fluxnet  
612 sites. Second, averaged across the Fluxnet sites, the Fluxnet mean SH is close to that of MERRA-  
613 Land, and above that of MERRA-2 (by  $6 \text{ Wm}^{-2}$ , 18 %). In contrast, for the global averages in  
614 Section 3.a the reference data sets were all close to MERRA-2 (and MERRA), with MERRA-Land  
615 standing out as being biased high.

616 Figure 10 shows the JJA  $R_{anom}$  averaged over the 20 Fluxnet sites for each reanalyses vs. each of  
617 Fluxnet, GLEAM, and MTE, with the global average JJA  $R_{anom}$  from Section 3.d also included for  
618 GLEAM and MTE. The  $R_{anom}$  for the Fluxnet data are quite low, which is somewhat expected due  
619 to the mismatch in spatial representation between the tower-based observations and the reanalysis.  
620 Nonetheless, the Fluxnet  $R_{anom}$  (as well as the GLEAM and MTE  $R_{anom}$  at the same locations)  
621 indicates similar relative reanalysis performance as the global mean  $R_{anom}$ . In particular, for LH  
622 MERRA-2 and MERRA-Land outperform MERRA, as also indicated by the global means. How-  
623 ever, the one discrepancy is that the  $R_{anom}$  vs. the Fluxnet data is similar for ERA-Interim and  
624 MERRA-2, while the global comparisons (and also the GLEAM and MTE data averaged across  
625 the Fluxnet sites) all suggest that ERA-Interim outperforms MERRA-2 (giving mean  $R_{anom}$  around  
626 0.1 higher). For SH, the rank order between the average JJA  $R_{anom}$  is the same from the Fluxnet  
627 data than from the global reference data sets, with the MERRA-Land  $R_{anom}$  again being lower than

628 that for MERRA (and MERRA-2), and the ERA-Interim average  $R_{anom}$  being higher than that for  
629 MERRA-2.

630 It is notable that over the Fluxnet tower sites, both GLEAM and MTE have higher average  $R_{anom}$   
631 with the reanalyses than the Fluxnet observations do. In particular, MTE was trained on an earlier  
632 generation of the Fluxnet data, and the higher mean  $R_{anom}$  vs. MTE than vs. Fluxnet suggests that  
633 the MTE algorithm has added coarse-scale information (similar quality control was applied here  
634 as was applied to the tower observations used in MTE). For the interested reader, supplemental  
635 Figure 4 shows scatterplots of the MERRA-2 LH  $R_{anom}$  vs. each reference data set at the 20  
636 individual sites.

637 Note that for Fluxnet, the  $R_{anom}$  for (LH+SH), plotted in Figure 10c is consistently about 0.1  
638 higher than the  $R_{anom}$  for either LH or SH separately. Decker et al. (2012) obtained a similar  
639 result for the correlation between reanalyses and tower observations. This indicates that the eddy  
640 covariance measurements and the reanalyses have a stronger agreement in the implied incoming  
641 radiation than in the partitioning of that radiation into LH and SH (this result is unchanged if the  
642  $R_{anom}$  are calculated from the Fluxnet data that have not been energy balance-corrected ). This  
643 could be a signal of errors in the partitioning within the reanalyses, or perhaps just as likely,  
644 this difference is associated with the spatial representation of the tower observations, since the  
645 incoming radiation is more spatially homogeneous than either LH or SH on its own.

#### 646 *f. Precipitation Corrections and Air Temperature Performance*

647 Finally, we seek to establish whether the precipitation corrections in MERRA-2 influenced the  
648 local  $T_{max}^{2m}$ . We do this by comparing the performance of the MERRA-2 and MERRA  $T_{max}^{2m}$  to  
649 Figure 3c, which shows the MERRA-2 sensitivity to observed precipitation. Figure 11 shows the  
650  $T_{max}^{2m} R_{anom}$  vs. CRU observations over JJA for MERRA-2 and MERRA. In general, the MERRA-

651  $2 R_{anom}$  is high ( $> 0.7$ ) across most of the domain, particularly in the high latitudes, with much  
 652 lower ( $< 0.4$ ) values across much of the tropics and parts of South America, Africa, and south  
 653 Asia. Note that the latter regions all have relatively sparsely distributed CRU station data, which is  
 654 likely contributing to the lower agreement with the reanalyses. Compared to MERRA, the greatest  
 655 improvements in the MERRA-2  $T_{max}^{2m} R_{anom}$  occurred in the eastern US, much of tropical South  
 656 America and Africa, the Sahel, and parts of south Asia and China. There are also several regions  
 657 where the  $T_{max}^{2m} R_{anom}$  is reduced, including northern South America, and much of southeast Asia.  
 658 Overall, the global averaged  $T_{max}^{2m} R_{anom}$  vs. CRU was increased from 0.69 for MERRA to 0.75 for  
 659 MERRA-2.

660 Comparing Figure 11c to Figure 3c, the regions with the strongest sensitivity of  $T_{max}^{2m}$  to the  
 661 precipitation corrections generally have relatively large changes in the  $T_{max}^{2m} R_{anom}$  (including the  
 662 Sahel, parts of south Asia, and central America). Consequently, where the metric in Figure  
 663 3c is above 0.25 (i.e., the observation-corrected precipitation explains at least 25% more of the  
 664 MERRA-2  $T_{max}^{2m}$  variance than the model-generated precipitation does), the area-averaged absolute  
 665 change in the  $R_{anom}$  is 0.15, compared to an area-average absolute change of 0.07 elsewhere. This  
 666 tendency toward relatively large change in the  $T_{max}^{2m} R_{anom}$  where  $T_{max}^{2m}$  is sensitive to the precipita-  
 667 tion corrections suggests that the observed precipitation in MERRA-2 contributed to the change in  
 668  $T_{max}^{2m}$  performance. Additionally, the change in  $T_{max}^{2m} R_{anom}$  in these regions is generally, although  
 669 not always, positive (giving an area averaged change in the  $R_{anom}$  of 0.06 where the metric in Fig-  
 670 ure 3c is greater than 0.25). In some of the instances where the  $T_{max}^{2m} R_{anom}$  is degraded, this can be  
 671 traced back to errors in the precipitation observation data sets input into MERRA-2. For example,  
 672 over Myanmar, the  $T_{max}^{2m} R_{anom}$  is decreased by more than 0.15, likely due to persistent local errors  
 673 in the precipitation observations input into MERRA-2 (Reichle et al. 2017b). Finally, there are  
 674 also regions with large changes in the  $T_{max}^{2m} R_{anom}$  outside of the regions of  $T_{max}^{2m}$  sensitivity to pre-

675 cipation (the eastern US, tropical Africa and South America, and central China). The  $T_{max}^{2m} R_{anom}$   
676 is increased in MERRA-2 across most of these regions, likely due to other advances (beyond the  
677 use of observed precipitation) in the MERRA-2 modeling and assimilation system.

#### 678 4. Summary and conclusions

679 The land surface energy budgets of three reanalyses from NASA (MERRA, MERRA-Land, and  
680 MERRA-2) are compared here to the best available estimates from the literature and to (largely)  
681 independent global reference data sets. In terms of the global land annual averages, the results sug-  
682 gest that the MERRA-2 LH and SH are biased high by  $5 \text{ Wm}^{-2}$  and  $6 \text{ Wm}^{-2}$ , respectively, while  
683  $SW_u$  has a large positive bias of  $14 \text{ Wm}^{-2}$ ,  $SW_d$  is biased high by  $3 \text{ Wm}^{-2}$ , and the upwelling and  
684 downwelling LW components are biased low, by  $11 \text{ Wm}^{-2}$  and  $13 \text{ Wm}^{-2}$ , respectively. Compared  
685 to MERRA, this is a slight ( $\sim 2 \text{ Wm}^{-2}$ ) reduction in the LH and  $SW_{net}$  biases, while the difference  
686 is even smaller for the LW terms ( $\sim 1 \text{ Wm}^{-2}$ ). The radiation biases are associated with known  
687 issues in the GEOS-5 models used in the reanalyses, specifically a tendency to underestimate mid-  
688 latitude continental clouds (Wang and Dickinson 2013) and a cool bias in the model  $T_{skin}$  (Draper  
689 et al. 2015).

690 Compared to reference flux estimates from GLEAM and MTE over the Boreal summer (when  
691 both the fluxes themselves and their biases are greatest), the largest MERRA-2 LH biases ( $>20$   
692  $\text{Wm}^{-2}$ , vs. either GLEAM or MTE) occur in regions where LH is energy-limited, such as in the  
693 high latitudes, the tropics, parts of south Asia, and the eastern US. The MERRA-2 LH biases are  
694 typically smaller in regions where LH is moisture-limited, which include the drier regions of the  
695 mid and low latitudes. In some of these moisture-limited regions (parts of south Asia and Mexico)  
696 the high bias in the MERRA LH was largely removed in MERRA-2 (and MERRA-Land), likely  
697 because the observed precipitation used in the latter was lower than that produced by the MERRA



698 (or MERRA-2) modeling systems. Finally, comparison to the evaporative fraction from MTE and  
699 to  $R_{net}$  from CERES-EBAF or as inferred from MTE LH+SH indicates that the regional biases in  
700 the reanalyses LH are generally associated with differences in the partitioning of  $R_{net}$  into LH and  
701 SH rather than with differences in the radiation input.

702 The temporal agreement between the reanalyses and the reference data sets over Boreal summer  
703 was measured using the monthly anomaly correlation ( $R_{anom}$ ) over JJA. For LH, the  $R_{anom}$  between  
704 the reanalyses and the reference data sets (GLEAM and MTE) again showed some dependency  
705 on the LH regime, with a tendency towards better agreement where LH is moisture-limited than  
706 where it is energy-limited. The lower agreement in energy-limited regions does not necessarily  
707 imply poorer performance in the reanalyses, as it may be due to errors in the reference data  
708 sets. The globally averaged  $R_{anom}$  values show the expected improvement in skill with each new  
709 NASA reanalyses. For example, MERRA-2 has slightly better globally averaged LH  $R_{anom}$  (0.48  
710 vs GLEAM) than MERRA-Land (0.45), which is substantially better than MERRA (0.39). The  
711  $R_{anom}$  was also calculated for the monthly mean daily  $T_{max}^{2m}$  vs. CRU reference data over JJA. Av-  
712 eraged over global land, the JJA  $T_{max}^{2m}$   $R_{anom}$  vs. CRU increased from 0.69 for MERRA to 0.75  
713 for MERRA-2. The results presented above for the regional biases and  $R_{anom}$  were based on the  
714 Boreal summer, however the same analysis has been performed over the Austral summer (not  
715 shown), yielding qualitatively similar results.

716 The use of observed precipitation in MERRA-2 was motivated by the hope that the subsequent  
717 improvements in simulated soil moisture would lead to the improved partitioning of incoming  
718 radiation between latent and sensible heating, ultimately leading to improvements in the diurnal  
719 evolution of the boundary layer. It is difficult, however, to unequivocally attribute the improve-  
720 ments in MERRA-2 to the use of observed precipitation because MERRA-2 includes many other  
721 modeling and assimilation advances relative to MERRA. Nonetheless, many of the improvements

722 in the MERRA-2 LH and  $T^{2m}$  are consistent with the changes expected from the use of observed  
 723 precipitation. MERRA-2 and MERRA-Land have smaller positive LH biases and higher LH  $R_{anom}$   
 724 than MERRA in regions where LH is moisture-limited and thus sensitive to precipitation (south  
 725 Asia and the western US). This is most easily explained by the forcing of the land surface with ob-  
 726 served precipitation in MERRA-2. Additionally, regions where the MERRA-2 JJA  $T_{max}^{2m}$  was most  
 727 sensitive to the precipitation corrections (the Sahel, central US, and parts of south Asia), generally  
 728 experience larger changes in the  $T_{max}^{2m} R_{anom}$  from MERRA to MERRA-2. However, the changes  
 729 in  $R_{anom}$  in these areas are not uniformly positive, and in some cases degraded  $T_{max}^{2m} R_{anom}$  can be  
 730 traced back to problems in the input precipitation data sets (e.g., over Myanmar). In the future, the  
 731 use of precipitation corrections could be enhanced by also implementing a land data assimilation  
 732 scheme to update the model soil moisture according to observations (e.g., Draper et al. (2011);  
 733 Dharssi et al. (2011); De Lannoy and Reichle (2016)). By making use of remotely sensed obser-  
 734 vations, the land data assimilation would be particularly valuable in regions where the rain-gauge  
 735 network is sparse or has known problems (e.g., in Africa and parts of southeast Asia).

736 However, some of the largest biases and lowest  $R_{anom}$  for the MERRA-2 turbulent fluxes occur  
 737 where the LH is energy-limited and thus less sensitive to improvements in the precipitation and  
 738 soil moisture. Hence, future efforts to improve the MERRA-2 land surface turbulent fluxes would  
 739 best be focused on other facets of the modeling and assimilation. Specifically, future GEOS-5  
 740 development should focus on the overestimated evaporative fraction where LH is energy-limited.  
 741 Additionally, even though the MERRA-2  $R_{net}$  is relatively unbiased (compared to CERES-EBAF),  
 742 there are large compensating biases in the individual SW and LW radiation fluxes that are 2-3 times  
 743 the magnitude of the LH biases in terms of the global land annual averages. Reducing the cloud  
 744 bias in the atmospheric model will help these biases, as will re-defining the model  $T_{skin}$  to generate  
 745 a  $LW_u$  more consistent with observations.

746 Finally, the SH results for MERRA-Land are troubling. While MERRA-Land did have the  
 747 desired reduction in the LH biases compared to MERRA (to  $1 \text{ Wm}^{-2}$  in the global land annual  
 748 average), it also had a compensating, and much larger, increase in the SH bias (up to  $15 \text{ Wm}^{-2}$   
 749 in the global land average). Additionally, the JJA  $R_{anom}$  compared to MTE were reduced from  
 750 MERRA to MERRA-Land (from a global average of 0.36 to 0.28), despite the LH  $R_{anom}$  being  
 751 increased. The cause of the degraded SH in MERRA-Land is presently unknown, but given the  
 752 otherwise similar MERRA and MERRA-Land land surface models and meteorological forcing,  
 753 an obvious possibility is that the use of observed precipitation in an offline (land-only) replay of  
 754 an analysis, such as MERRA-Land, can lead to inconsistencies in the forcing (e.g., warm and dry  
 755 air, stemming from dry conditions in MERRA, overlying cold ground induced by high antecedent  
 756 rainfall from the observations). Such inconsistencies would not appear in MERRA or (as much)  
 757 in MERRA-2, given the coupling in the reanalyses of the land surface state with the overlying  
 758 atmosphere.

759 While this work focused on evaluating surface energy fluxes in MERRA-2, the findings have  
 760 relevance to anyone interested in designing a methodology to evaluate global estimates of turbu-  
 761 lent heat fluxes. The gridded LH reference data sets (GLEAM and MTE) had better agreement  
 762 with the reanalyses time series (as measured by  $R_{anom}$ ), and were more useful for evaluating the  
 763 reanalysis output than were the tower observations. In particular they offer (near-) global cover-  
 764 age across several decades, at similarly course resolution to the reanalyses. In the absence of a  
 765 recognized truth for LH (or other similar terms), the recommended evaluation strategy is to com-  
 766 pare the product under evaluation to multiple data sets. However, given the uncertainty in the  
 767 available reference data sets, extra care is necessary to understand the methodology, input data,  
 768 assumptions, and potential dependencies and weaknesses of each reference data set. This process  
 769 relies on expert judgement and inevitably introduces some subjectivity into the interpretation of

770 the results. Further development of global gridded LH data sets (including the quality and quantity  
771 of ground-‘truth’ observations), to increase their confidence would obviously be of great benefit  
772 to this process.

773 The GLEAM and MTE reference data sets used here are independent of each other and are based  
774 on very different methodologies, thus providing complementary information for use in an evalua-  
775 tion. However, given the use of the common precipitation input data in GLEAM as in MERRA-2,  
776 and the fact that MTE data is not optimized to estimate interannual variability, LH estimates from  
777 a third reference data set would be useful. Emerging global and multi-decadal land surface flux  
778 data sets based on an energy balance approach (Anderson et al. 2011), or alternative observational  
779 frameworks (Alemohammad et al. 2017) would provide useful complements to GLEAM and MTE  
780 for a more comprehensive analysis.

781 *Acknowledgments.* Funding for this work was provided by the NASA Modeling, Analysis, and  
782 Prediction program. Computational resources were provided by the NASA High-End Computing  
783 Program through the NASA Center for Climate Simulation. The authors acknowledge the teams  
784 that produce and publish the GLEAM, MTE, CERES-EBAF, ERA-Interim, MERRA, MERRA-  
785 Land, and MERRA-2 products. Additionally, we are grateful to Diego Miralles (VU University  
786 Amsterdam/Ghent University), Martin Jung (Max Planck Institute for Biogeochemistry), and Seiji  
787 Kato (NASA Langley Research Center) for their thoughtful feedback on this work, and detailed  
788 advice on the use of GLEAM, MTE, and CERES-EBAF, respectively. The FLUXNET eddy co-  
789 variance data processing and harmonization was carried out by the European Fluxes Database  
790 Cluster, AmeriFlux Management Project, and Fluxdata project of FLUXNET, with the support of  
791 CDIAC and ICOS Ecosystem Thematic Center, and the OzFlux, ChinaFlux and AsiaFlux offices.

## References

- Alemohammad, S. H., and Coauthors, 2016: Water, Energy, and Carbon with Artificial Neural Networks (WECANN): A statistically-based estimate of global surface turbulent fluxes using solar-induced fluorescence. *Biogeosciences*, **15**, 4101–4124, doi:10.5194/bg-14-4101-2017.
- Anderson, M., and Coauthors, 2011: Mapping daily evapotranspiration at field to continental scales using geostationary and polar orbiting satellite imagery. *Hydrology and Earth System Sciences*, **15**, 223–239, doi:10.5194/hess-15-223-2011.
- Baldocchi, D., and Coauthors, 2001: FLUXNET: A new tool to study the temporal and spatial variability of ecosystem-scale carbon dioxide, water vapor, and energy flux densities. *Bulletin of the American Meteorological Society*, **82**, 2415–2434, doi:10.1175/1520-0477(2001)082<2415:FANTTS>2.3.CO;2.
- Beck, H., A. van Dijk, V. Levizzani, J. Schellekens, D. Miralles, B. Martens, and A. de Roo, 2017: MSWEP: 3-hourly 0.25° global gridded precipitation (1979–2015) by merging gauge, satellite, and reanalysis data. *Hydrology and Earth System Sciences*, **21**, 589–615, doi:10.5194/hess-21-589-2017.
- Betts, A., A. Tawfik, and R. Desjardins, 2017: Revisiting hydrometeorology using cloud and climate observations. *Journal of Hydrometeorology*, **18**, 939–955, doi:10.1175/JHM-D-16-0203.1.
- CERES-EBAF, 2017: CERES\_EBAF-Surface\_Ed4.0, Data Quality Summary (May 26, 2017). Accessed Jun. 20, 2017 pp., [https://ceres.larc.nasa.gov/documents/DQ\\_summaries/CERES\\_EBAF-Surface\\_Ed4.0\\_DQS.pdf](https://ceres.larc.nasa.gov/documents/DQ_summaries/CERES_EBAF-Surface_Ed4.0_DQS.pdf).

813 Chen, M., W. Shi, P. Xie, V. B. S. Silva, V. E. Kousky, R. Wayne Higgins, and J. E. Janowiak,  
814 2008: Assessing objective techniques for gauge-based analyses of global daily precipitation.  
815 *Journal of Geophysical Research: Atmospheres*, **113**, D04 110, doi:10.1029/2007JD009132.

816 De Lannoy, G., and R. Reichle, 2016: Assimilation of SMOS brightness temperatures or soil  
817 moisture retrievals into a land surface model. *Hydrology and Earth System Sciences*, **20**, 4895–  
818 4911, doi:10.5194/hess-20-4895-2016.

819 de Rosnay, P., G. Balsamo, C. Albergel, J. Munoz-Sabater, and L. Isaksen, 2014: Initialisation of  
820 land surface variables for numerical weather prediction. *Surveys in Geophysics*, **35**, 607–621,  
821 doi:10.1007/s10712-012-9207-x.

822 Decker, M., M. Brunke, Z. Wang, K. Sakaguchi, X. Zeng, and M. Bosilovich, 2012: Evaluation  
823 of the Reanalysis Products from GSFC, NCEP, and ECMWF Using Flux Tower Observations.  
824 *Journal of Climate*, **25**, 1916–1944, doi:10.1175/JCLI-D-11-00004.1.

825 Dee, D., and Coauthors, 2011: The ERA-Interim reanalysis: configuration and performance of the  
826 data assimilation system. *Quarterly Journal of the Royal Meteorological Society*, **137**, 553–597,  
827 doi:10.1002/qj.828.

828 Dharssi, I., K. Bovis, B. Macpherson, and C. Jones, 2011: Operational assimilation of ASCAT  
829 surface soil wetness at the Met Office. *Hydrology and Earth System Sciences*, **15**, 2729–2746,  
830 doi:10.5194/hess-15-2729-2011.

831 Draper, C., J.-F. Mahfouf, and J. Walker, 2011: Root-zone soil moisture from the assimilation  
832 of screen-level variables and remotely sensed soil moisture. *Journal of Geophysical Research*,  
833 **116**, D02 127, doi:10.1029/2010JD013829.

834 Draper, C., R. Reichle, and B. De Lannoy, G. and Scarino, 2015: A Dynamic Approach to Ad-  
 835 dressing Observation-Minus-Forecast Bias in a Land Surface Skin Temperature Data Assimila-  
 836 tion System. *Journal of Hydrometeorology*, **16**, 449–464, doi:10.1175/JHM-D-14-0087.1.

837 Fluxnet, 2015: FLUXNET2015 Dataset. Accessed Aug 9, 2016 pp.,  
 838 <http://fluxnet.fluxdata.org/data/fluxnet2015-dataset/>.

839 Gelaro, R., and Coauthors, 2015: Evaluation of the 7-km GEOS-5 Nature Run. 285pp pp., NASA  
 840 Technical Report Series on Global Modeling and Data Assimilation, NASA/TM-2014-104606,  
 841 Vol. 36.

842 Gelaro, R., and Coauthors, 2017: The Modern-Era Retrospective Analysis for Research and  
 843 Applications, Version 2 (MERRA-2). *Journal of Climate*, **30**, 5419–5454, doi:10.1175/  
 844 JCLI-D-16-0758.1.

845 Global Modeling and Assimilation Office, 2008a: tavg1\_2d\_slv\_Nx: MERRA 2D IAU Diagnostic,  
 846 Single Level Meteorology, Time Average 1-hourly V5.2.0. Goddard Earth Sciences Data and  
 847 Information Services Center (GES DISC), Greenbelt, MD, Accessed Oct 1, 2016 pp., doi:10.  
 848 5067/B6DQZQLSFDLH.

849 Global Modeling and Assimilation Office, 2008b: tavgM\_2d\_lnd\_Nx: MERRA 2D IAU Diagnos-  
 850 tic, Land Only States and Diagnostics, Monthly Mean V5.2.0. Goddard Earth Sciences Data  
 851 and Information Services Center (GES DISC), Greenbelt, MD, Accessed Oct 1, 2016 pp., doi:  
 852 10.5067/XOHTIIK0W9RK.

853 Global Modeling and Assimilation Office, 2008c: tavgM\_2d\_mld\_Nx: MERRA Simulated 2D  
 854 Incremental Analysis Update (IAU) MERRA-Land reanalysis, GEOSldas-MERRALand, Time

855 Average Monthly Mean V5.2.0. Goddard Earth Sciences Data and Information Services Center  
 856 (GES DISC), Greenbelt, MD, Accessed Oct 1, 2016 pp., doi:10.5067/K9PCGOMQ1XP1.

857 Global Modeling and Assimilation Office, 2015a: MERRA-2 tavg1\_2d\_lfo\_Nx: 2D, 1-Hourly,  
 858 Time-Averaged, Single-Level, Assimilation, Land Surface Forcings, V5.12.4. Goddard Earth  
 859 Sciences Data and Information Services Center (GES DISC), Greenbelt, MD, Accessed Oct 1,  
 860 2016 pp., doi:10.5067/L0T5GEG1NYFA.

861 Global Modeling and Assimilation Office, 2015b: MERRA-2 tavgM\_2d\_lnd\_Nx: 2D, Monthly  
 862 Mean, Time-Averaged, Single-Level, Assimilation, Land Surface Diagnostics, V5.12.4. God-  
 863 dard Earth Sciences Data and Information Services Center (GES DISC), Greenbelt, MD, Ac-  
 864 cessed Oct 1, 2016 pp., doi:10.5067/8S35XF81C28F.

865 Global Modeling and Assimilation Office, 2015c: MERRA-2 tavgM\_2d\_slv\_Nx: 2D, Monthly  
 866 Mean, Time-Averaged, Single-Level, Assimilation, Single-Level Diagnostics, V5.12.4. God-  
 867 dard Earth Sciences Data and Information Services Center (GES DISC), Greenbelt, MD, Ac-  
 868 cessed Oct 1, 2016 pp., doi:10.5067/AP1B0BA5PD2K.

869 Harris, I., P. Jones, T. Osborn, and D. Lister, 2014: Updated high-resolution grids of monthly  
 870 climatic observations - the CRU TS3.10 Dataset. *International Journal of Climatology*, **34**,  
 871 623642, doi:10.1002/joc.3711.

872 Huffman, G., R. Adler, D. Bolvin, and G. Gu, 2009: Improving the global precipitation  
 873 record: GPCP Version 2.1. *Geophysical Research Letters*, **36** (17), L17 808, doi:10.1029/  
 874 2009GL040000.

875 Jiménez, C., and Coauthors, 2011: Global intercomparison of 12 land surface heat flux estimates.  
 876 *Journal of Geophysical Research: Atmospheres*, **116**, D02 102, doi:10.1029/2010JD014545.



- 877 Jung, M., M. Reichstein, and A. Bondeau, 2009: Towards global empirical upscaling of  
878 FLUXNET eddy covariance observations: validation of a model tree ensemble approach us-  
879 ing a biosphere model. *Biogeosciences*, **6**, 2001–2013, doi:10.5194/bg-6-2001-2009.
- 880 Jung, M., and Coauthors, 2010: Recent decline in the global land evapotranspiration trend due to  
881 limited moisture supply. *Nature*, **467**, 951–954, doi:10.1038/nature09396.
- 882 Jung, M., and Coauthors, 2011: Global patterns of land-atmosphere fluxes of carbon diox-  
883 ide, latent heat, and sensible heat derived from eddy covariance, satellite, and meteoro-  
884 logical observations. *Journal of Geophysical Research - Biogeosciences*, **116**, G00j07, doi:  
885 10.1029/2010jg001566.
- 886 Kato, S., N. Loeb, F. Rose, D. Doelling, D. Rutan, T. Caldwell, L. Yu, and R. Weller, 2013: Surface  
887 Irradiances Consistent with CERES-Derived Top-of-Atmosphere Shortwave and Longwave Ir-  
888 radiances. *Journal of Climate*, **26**, 2719–2740, doi:10.1175/JCLI-D-12-00436.1.
- 889 Koster, R., G. Salvucci, A. Rigden, M. Jung, G. Collatz, and S. Schubert, 2015: The pattern across  
890 the continental United States of evapotranspiration variability associated with water availability.  
891 *Frontiers in Earth Science*, **3**, 35pp, doi:10.3389/feart.2015.00035.
- 892 Koster, R., and Coauthors, 2006: GLACE: The Global Land-Atmosphere Coupling Experiment.  
893 Part I: Overview. *Journal of Hydrometeorology*, **7**, 590–610, doi:10.1175/JHM510.1.
- 894 L'Ecuyer, T., and Coauthors, 2015: The observed state of the Energy budget in the early 21st  
895 Century. *Journal of Climate*, **28**, 8319–8346, doi:10.1175/JCLI-D-14-00556.1.
- 896 Martens, B., and Coauthors, 2017: GLEAM v3: satellite-based land evaporation and root-zone soil  
897 moisture. *Geoscientific Model Development*, **10**, 1903–1925, doi:10.5194/gmd-10-1903-2017.

898 Miralles, D., T. Holmes, R. de Jeu, J. Gash, A. Meesters, and A. Dolman, 2011: Global land-  
 899 surface evaporation estimated from satellite-based observations. *Hydrology and Earth System*  
 900 *Sciences*, **15**, 453–469, doi:10.5194/hess-15-453-2011.

901 Miralles, D., M. van den Berg, A. Teuling, and R. de Jeu, 2012: Soil moisture-temperature cou-  
 902 pling: A multiscale observational analysis. *Geophysical Research Letters*, **39**, L21 707, doi:  
 903 10.1029/2012GL053703.

904 Molod, A., L. Takacs, M. Suarez, and J. Bacmeister, 2015: Development of the GEOS-5 atmo-  
 905 spheric general circulation model: evolution from MERRA to MERRA-2. *Geoscientific Model*  
 906 *Development*, **8**, 1339–1356, doi:10.5194/gmd-8-1339-2015.

907 Molod, A., L. Takacs, M. Suarez, J. Bacmeister, I.-S. Song, and A. Eichmann, 2012: The GEOS-5  
 908 atmospheric general circulation model: Mean climate and development from MERRA to For-  
 909 tuna . 117pp pp., NASA Technical Report Series on Global Modeling and Data Assimilation,  
 910 NASA/TM-2014-104606, Vol. 28.

911 Mueller, B., and Coauthors, 2011: Evaluation of global observations-based evapotranspiration  
 912 datasets and IPCC AR4 simulations. *Geophysical Research Letters*, **38**, L06 402, doi:10.1029/  
 913 2010GL046230.

914 Mueller, B., and Coauthors, 2013: Benchmark products for land evapotranspiration: LandFlux-  
 915 EVAL multi-data set synthesis. *Hydrology and Earth System Sciences*, **17**, 3707–3720, doi:  
 916 10.5194/hess-17-3707-2013.

917 NSIT, 2007: A NASA Earth science implementation plan for energy and water cycle research:  
 918 Predicting energy and water cycle consequences of Earth system variability and change. 89pp  
 919 pp., [http://news.cisc.gmu.edu/doc/NEWS\\_implementation.pdf](http://news.cisc.gmu.edu/doc/NEWS_implementation.pdf).

Reichle, R., C. Draper, Q. Liu, M. Girotto, S. Mahanama, R. Koster, and G. D. Lannoy, 2017a: Assessment of MERRA-2 land surface hydrology estimates. *Journal of Climate*, **30**, 2937–2960, doi:10.1175/JCLI-D-16-0720.1.

Reichle, R., R. Koster, G. De Lannoy, B. Forman, Q. Liu, S. Mahanama, and A. Toure, 2011: Assessment and enhancement of MERRA land surface hydrology estimates. *Journal of Climate*, **24**, 6322–6338, doi:10.1175/JCLI-D-10-05033.1.

Reichle, R., and Q. Liu, 2014: Observation-corrected precipitation estimates in GEOS-5. 18pp pp., NASA Technical Report Series on Global Modeling and Data Assimilation, NASA/TM-2014-104606, Vol. 35.

Reichle, R., Q. Liu, R. Koster, C. Draper, S. Mahanama, and G. Partyka, 2017b: Land surface precipitation in MERRA-2. *Journal of Climate*, **30**, 1643–1664, doi:10.1175/JCLI-D-16-0570.1.

Rienecker, M., and Coauthors, 2011: MERRA - NASA's Modern-Era Retrospective Analysis for Research and Applications. *Journal of Climate*, **24**, 3624–3648, doi:10.1175/JCLI-D-11-00015.1.

Schlosser, C., and X. Gao, 2010: Assessing evapotranspiration estimates from the Second Global Soil Wetness Project (GSWP-2) simulations. *Journal of Hydrometeorology*, **11**, 880–897, doi:10.1175/2010JHM1203.1.

Trenberth, K., J. Fasullo, and J. Kiehl, 2009: Earth's global energy budget. *Bulletin of the American Meteorological Society*, **90**, 311–323, doi:10.1175/2008BAMS2634.1.

University of East Anglia Climatic Research Unit, Harris I, and Jones, P, 2014: CRU TS3.22: Climatic Research Unit (CRU) Time-Series (TS) Version 3.22 of High Resolution Gridded Data

of Month-by-month Variation in Climate (Jan. 1901- Dec. 2013). NCAS British Atmospheric Data Centre, doi:10.5285/18BE23F8-D252-482D-8AF9-5D6A2D40990C.

Wang, K., and R. Dickinson, 2013: Global atmospheric downward longwave radiation at the surface from ground-based observations, satellite retrievals, and reanalyses. *Reviews of Geophysics*, **51**, 150–185, doi:10.1002/rog.20009.

Wild, M., D. Folini, and M. Hakuba, 2015: The energy balance over land and oceans: an assessment based on direct observations and CMIP5 climate models. *Clim Dyn*, **44**, 3393–3429, doi:10.1007/s00382-014-2430-z.

Wilson, K., and Coauthors, 2002: Energy balance closure at FLUXNET sites. *Agricultural and Forest Meteorology*, **113**, 223–243, doi:10.1016/S0168-1923(02)00109-0.

Xie, P., and P. Arkin, 1997: Global precipitation: A 17-year monthly analysis based on gauge observations, satellite estimates, and numerical model outputs. *Bulletin of the American Meteorological Society*, **78**, 2539–2558, doi:10.1175/1520-0477(1997)078<2539:GPAYMA>2.0.CO;2.

955	<b>LIST OF TABLES</b>	
956	<b>Table 1.</b> The reanalyses . . . . .	46
957	<b>Table 2.</b> The gridded reference data sets. . . . .	47
958	<b>Table 3.</b> Global annual land average energy budget from the NASA reanalyses ( $Wm^{-2}$ ),	
959	estimated over an area of 130.2 million km <sup>2</sup> . . . . .	48

TABLE 1. The reanalyses

Data set	Variables used	Output coverage and resolution (variable data set citation, where available)
MERRA-2	LH,SH, $LW_{net}$ , $SW_{net}$ $LW_d$ $T_{max}^{2m}$ , $T_{min}^{2m}$	1980-ongoing, hourly, $5/8^\circ \times 0.5^\circ$ global land (Global Modeling and Assimilation Office 2015b) global surface (Global Modeling and Assimilation Office 2015a) global surface (Global Modeling and Assimilation Office 2015c)
MERRA-Land	LH, SH, $LW_{net}$	1980-2016, hourly, $2/3^\circ \times 0.5^\circ$ global land (Global Modeling and Assimilation Office 2008c)
MERRA	LH,SH, $LW_{net}$ , $SW_{net}$ $LW_d$ $T_{max}^{2m}$ , $T_{min}^{2m}$	1979-2015, hourly, $2/3^\circ \times 0.5^\circ$ global land (Global Modeling and Assimilation Office 2008b) global surface (-) global surface (Global Modeling and Assimilation Office 2008a)
ERA-Interim	LH, SH	1979 - ongoing, monthly mean, 79 km global surface

TABLE 2. The gridded reference data sets.

Data set	Variables used	Output coverage and resolution	Dependencies, error estimates where available
GLEAM v3.1a	LH	1980-2016, daily mean, $0.25^\circ$ global land	Uses a precipitation data set that includes CPCU (used in MERRA-2, MERRA-Land) and ERA-Interim precipitation, uses $T^{2m}$ and radiation from ERA-Interim. <i>c.f.</i> tower obs., average ubRMSE: $20 \text{ Wm}^{-2}$ , average $R_{anom}$ : 0.42. Full details: Section 2.c.1.
MTE	LH, SH	1982-2011 monthly mean, $0.5^\circ$ global land, excluding non-vegetated regions	Trained on an earlier generation of the Fluxnet-2015 data set. Uses a CRU-based $T^{2m}$ data set, and CPCU precipitation (neither strongly influences temporal behavior). <i>c.f.</i> withheld tower obs., average RMSE: $15 \text{ Wm}^{-2}$ (LH & SH), average $R_{anom}$ 0.57 (LH), 0.60 (SH). Full details: Section 2.c.2.
CRU v4.00	$T_{min}^{2m}, T_{max}^{2m}$	1901-2015 monthly means $0.5^\circ$ global land (data not informed by station obs. have been removed)	Input station obs. will overlap with $T^{2m}$ assimilated into ERA-Interim. Locally, will be more uncertain where input station obs. are sparse. Full details: Section 2.c.3.
CERES-EBAF, vn 4.0	$SW_d, SW_u, LW_d, LW_u$	Mar. 2000-Feb. 2016 monthly mean, $1^\circ$ global surface	Uses atmospheric profile and $T_{skin}$ from same system as used in the NASA re-analyses (results in strong dependence for $LW_u, LW_d$ ). <i>c.f.</i> ground obs. average RMSE: $12 \text{ Wm}^{-2}$ ( $SW_d$ ), $10 \text{ Wm}^{-2}$ ( $LW_d$ ). Full details: Section 2.c.4.

960      TABLE 3. Global annual land average energy budget from the NASA reanalyses ( $Wm^{-2}$ ), estimated over an  
961      area of 130.2 million  $km^2$ .

	$SW_d$	$SW_u$	$LW_d$	$LW_u$	$R_{net}$	LH	SH
MERRA-2	204.6	40.7	312.6	385.5	91.0	47.8	42.2
MERRA-Land	as for MERRA			384.1	95.1	42.5	52.1
MERRA	206.5	40.9	313.7	386.7	92.6	50.4	41.2



## LIST OF FIGURES

962	<b>LIST OF FIGURES</b>	
963	<b>Fig. 1.</b>	The global annual mean energy budget over land from the reanalyses (MERRA-2 (M-2);
964		MERRA-Land (M-L); MERRA (M)), the literature (NEWS (NEW), Trenberth et al. (2009)
965		(Tre), Wild et al. (2015) (Wil), Jiménez et al. (2011) (Jim), Mueller et al. (2011) (Mu1), and
966		Mueller et al. (2013) (Mu3)), and the gridded reference data sets (MTE, GLEAM (GLM),
967		and CERES (CER)), for a) LH, b) SH, c) $SW_d$ , d) $SW_u$ , e) $LW_d$ , f) $LW_u$ , and g) $R_{net}$ . For
968		NEW, Tre, and Wil, the land mean has been approximated from published continental means
969		as described in Section 2.b. Error bars are included where provided, for NEW and Wil these
970		span the possible range described by multiple products, and for Jim and Mu1 these represent
971		one standard deviation across multiple products (see citations for full details). . . . . 51
972	<b>Fig. 2.</b>	$R_{anom}^2$ between monthly anomalies of LH and rootzone soil moisture (SM) in MERRA-2 for
973		JJA. No value is plotted where the correlation is negative. . . . . 52
974	<b>Fig. 3.</b>	JJA sensitivity of the monthly mean $T_{max}^{2m}$ to precipitation in MERRA-2: $R_{anom}^2$ between
975		the monthly mean $T_{max}^{2m}$ anomalies, and the two-monthly (current + previous months) pre-
976		cipitation anomalies, for (a) the model-generated precipitation (PRECTOT), and (b) the
977		observation-corrected precipitation (PRECTOTCORR), together with their difference (c)
978		$\Delta R_{anom}^2 = R_{anom}^2(\text{PRECTOTCORR}, T_{max}^{2m}) - R_{anom}^2(\text{PRECTOT}, T_{max}^{2m})$ . Values are plotted only
979		where the correlation between $T_{max}^{2m}$ and precipitation is negative. . . . . 53
980	<b>Fig. 4.</b>	The mean JJA turbulent fluxes, with GLEAM LH (column 1), MTE LH (column 2), and
981		MTE SH (column 3) reference data in row 1, and the difference from the reference data for
982		MERRA-2, MERRA-Land, and MERRA, in rows 2-4. The statistics span 1980-2016 for
983		GLEAM, and 1982-2011 for MTE. . . . . 54
984	<b>Fig. 5.</b>	Separation of mean JJA turbulent flux into evaporative fraction (EF) and incoming radia-
985		tion biases, with the MTE EF (column 1), MTE LH+SH (column 2), and CERES-EBAF
986		(column 3) reference data in row 1, and the difference from the reference data for MERRA-
987		2, MERRA-Land, and MERRA in rows 2-4. The statistics span 1982-2011 for MTE, and
988		2000-2015 for CERES-EBAF. . . . . 55
989	<b>Fig. 6.</b>	The mean JJA radiation terms, from the CERES-EBAF reference data (row 1), and differ-
990		ence from the reference data for MERRA-2 (row 1), for (columns 1-3) $SW_{net}$ , $LW_u$ , and $LW_d$ .
991		The statistics span 2000-2015. . . . . 56
992	<b>Fig. 7.</b>	The mean JJA $T^{2m}$ , from CRU reference data (row 1), and the difference from the reference
993		data for MERRA and MERRA-2 (rows 2-3), for the $T_{min}^{2m}$ (column 1), $T_{max}^{2m}$ (column 2), and
994		the DTR (column 3). The statistics span 1980-2015, and white plotted over land indicates
995		insufficient CRU data. . . . . 57
996	<b>Fig. 8.</b>	$R_{anom}$ between GLEAM LH, MTE LH, and MTE SH (columns 1-3) for MERRA, MERRA-
997		Land, MERRA-2, and ERA-Interim (rows 1-4), for JJA. Statistics span 1980-2016 for
998		GLEAM and 1982-2011 for MTE. . . . . 58
999	<b>Fig. 9.</b>	Bar plot of the mean annual (a) LH and (b) SH, across the 20 Fluxnet site locations, from
1000		MERRA-2 (M-2), MERRA-Land (M-L), MERRA (M), Fluxnet (FIN), MTE, and GLEAM
1001		(GLM; LH only), calculated using each data set at its native resolution (and screened tem-
1002		porally for Fluxnet availability). For the global data sets, circles are plotted for the global
1003		land annual mean (taken from Figure 1). . . . . 59

1004	<b>Fig. 10.</b>	Bar plot of the $R_{anom}$ over JJA averaged across the 20 Fluxnet site locations, for (a) LH,	
1005		(b) SH, and (c) LH+SH, between each pair of the reanalyses (MERRA-2 (M-2), MERRA-	
1006		Land (M-L), MERRA (M), and ERA-I (E-I)) and the reference data (Fluxnet (FIN), MTE,	
1007		and GLEAM (GLM)). The $R_{anom}$ vs. the Fluxnet reference data use the reanalysis output at	
1008		their reported spatial resolution (and screened temporally for Fluxnet availability), while the	
1009		$R_{anom}$ vs. GLEAM and MTE use reanalyses and reference data regridded to $1^\circ$ . For GLEAM	
1010		and MTE, circles are plotted for the global mean JJA $R_{anom}$ (averaged over subplots of Figure	
1011		8). . . . .	60
1012	<b>Fig. 11.</b>	The (a) MERRA-2 $R_{anom}$ vs. CRU monthly mean $T_{max}^{2m}$ , and (b) the improvement in the $T_{max}^{2m}$	
1013		$R_{anom}$ from MERRA to MERRA-2, both over JJA. Statistics span 1980-2015, and white	
1014		plotted over land indicates insufficient CRU data. . . . .	61

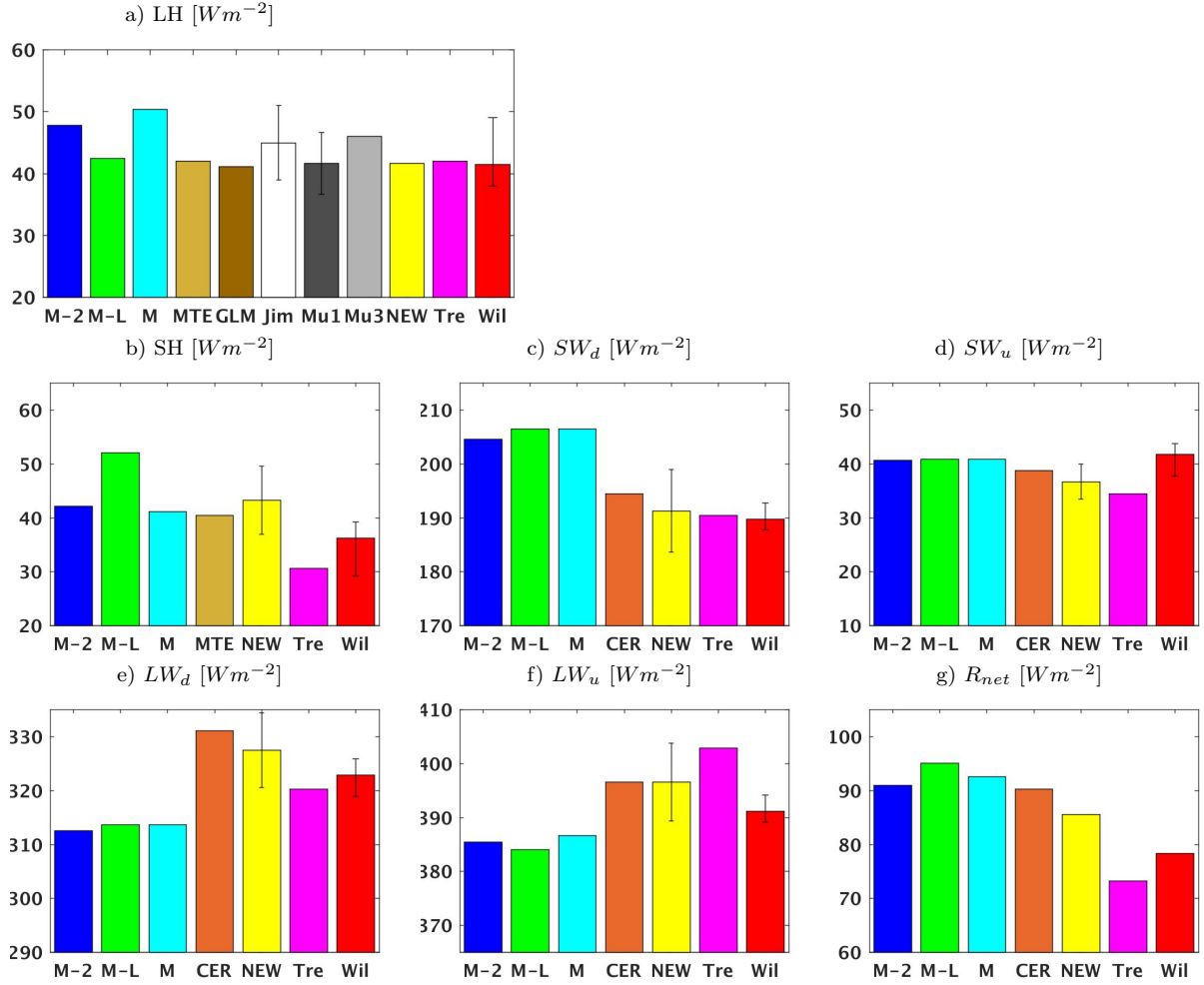


FIG. 1. The global annual mean energy budget over land from the reanalyses (MERRA-2 (M-2); MERRA-Land (M-L); MERRA (M)), the literature (NEWS (NEW), Trenberth et al. (2009) (Tre), Wild et al. (2015) (Wil), Jiménez et al. (2011) (Jim), Mueller et al. (2011) (Mu1), and Mueller et al. (2013) (Mu3)), and the gridded reference data sets (MTE, GLEAM (GLM), and CERES (CER)), for a) LH, b) SH, c)  $SW_d$ , d)  $SW_u$ , e)  $LW_d$ , f)  $LW_u$ , and g)  $R_{net}$ . For NEW, Tre, and Wil, the land mean has been approximated from published continental means as described in Section 2.b. Error bars are included where provided, for NEW and Wil these span the possible range described by multiple products, and for Jim and Mu1 these represent one standard deviation across multiple products (see citations for full details).

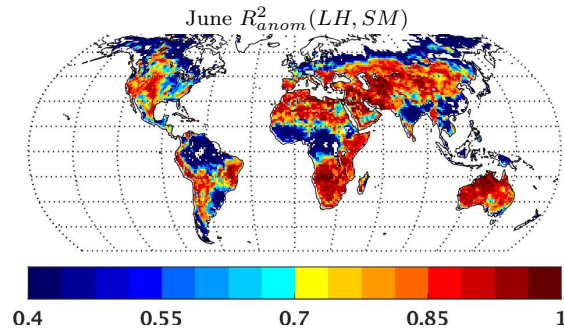


FIG. 2.  $R^2_{anom}$  between monthly anomalies of LH and rootzone soil moisture (SM) in MERRA-2 for JJA. No value is plotted where the correlation is negative.

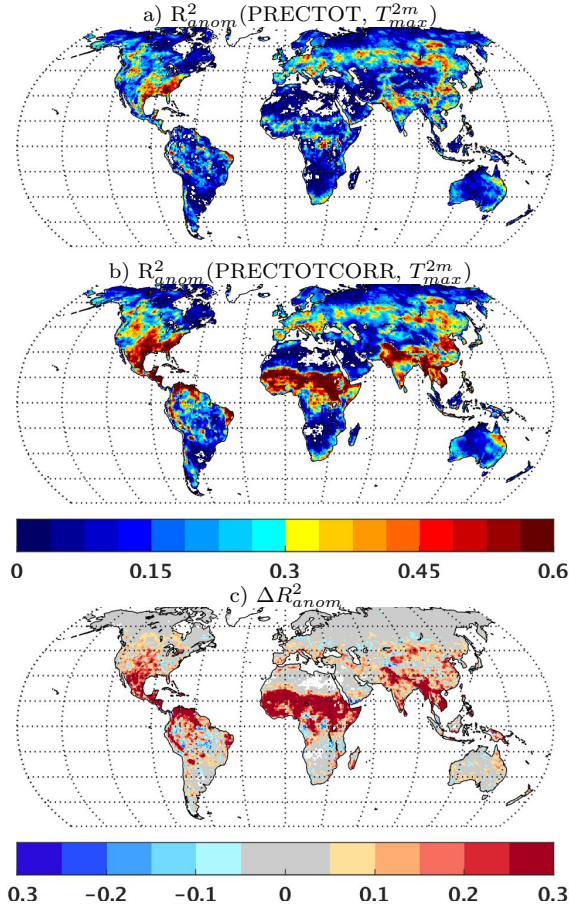


FIG. 3. JJA sensitivity of the monthly mean  $T_{max}^{2m}$  to precipitation in MERRA-2:  $R_{anom}^2$  between the monthly mean  $T_{max}^{2m}$  anomalies, and the two-monthly (current + previous months) precipitation anomalies, for (a) the model-generated precipitation (PRECTOT), and (b) the observation-corrected precipitation (PRECTOTCORR), together with their difference (c)  $\Delta R_{anom}^2 = R_{anom}^2(\text{PRECTOTCORR}, T_{max}^{2m}) - R_{anom}^2(\text{PRECTOT}, T_{max}^{2m})$ . Values are plotted only where the correlation between  $T_{max}^{2m}$  and precipitation is negative.

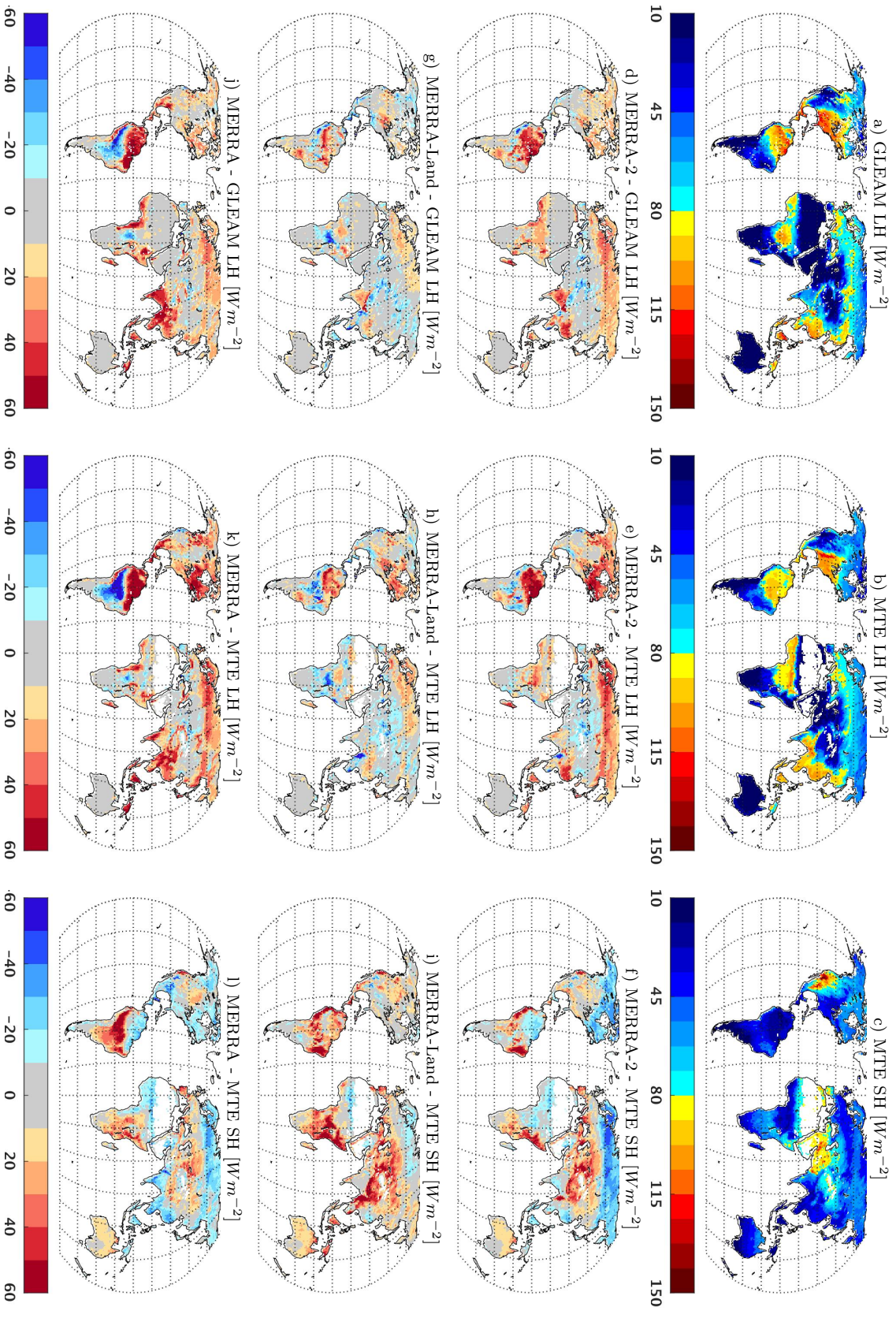


FIG. 4. The mean JJA turbulent fluxes, with GLEAM LH (column 1), MTE LH (column 2), and MTE SH (column 3) reference data in row 1, and the difference from the reference data for MERRA-2, MERRA-Land, and MERRA, in rows 2-4. The statistics span 1980-2016 for GLEAM, and 1982-2011 for MTE.



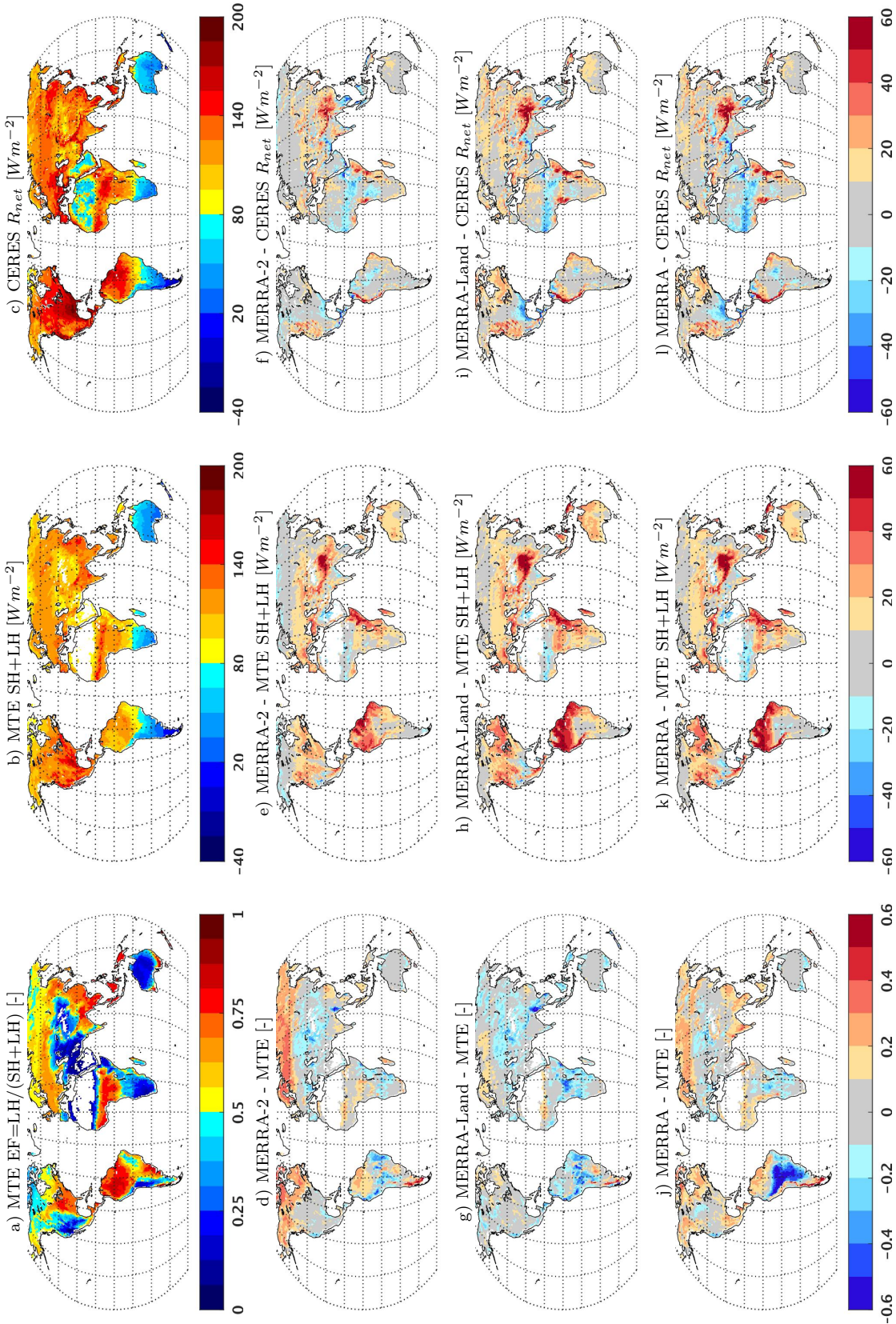


FIG. 5. Separation of mean JJA turbulent flux into evaporative fraction (EF) and incoming radiation biases, with the MTE EF (column 1), MTE LH+SH (column 2), and CERES-EBAF (column 3) reference data in row 1, and the difference from the reference data for MERRA-2, MERRA-Land, and MERRA in rows 2-4. The statistics span 1982-2011 for MTE, and 2000-2015 for CERES-EBAF.

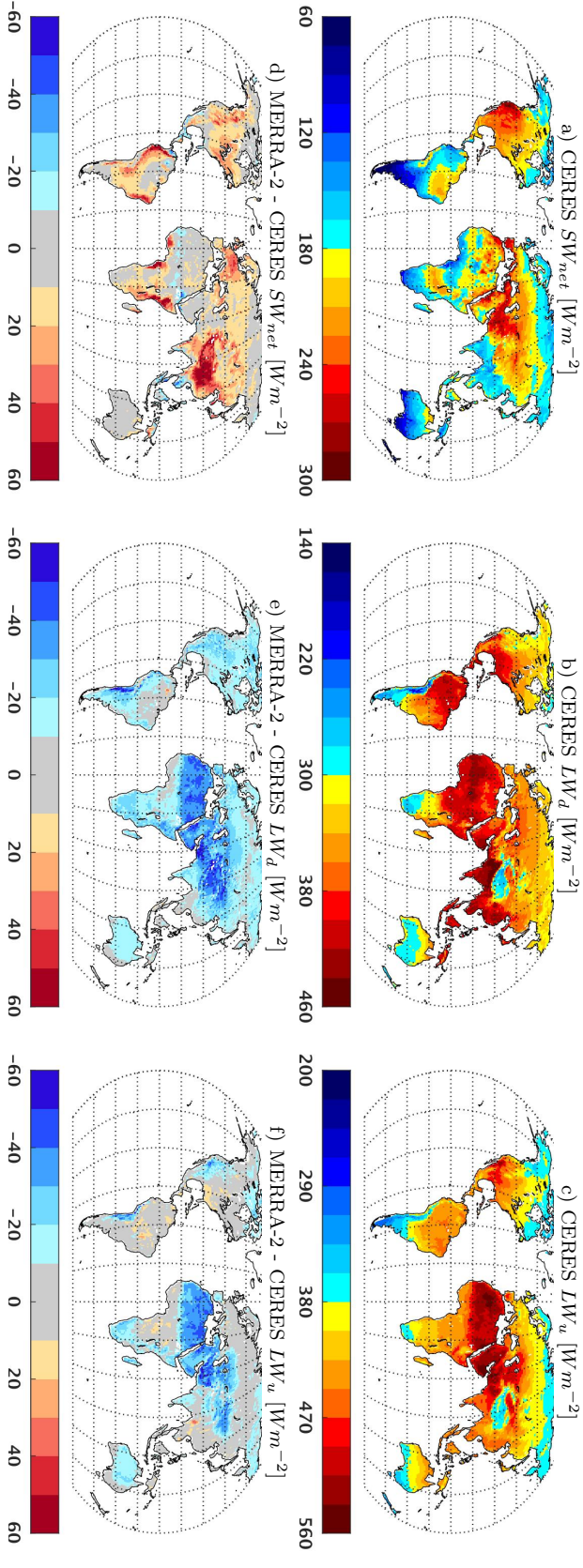


FIG. 6. The mean JJA radiation terms, from the CERES-EBAF reference data (row 1), and difference from the reference data for MERRA-2 (row 1),  
for (columns 1-3)  $SW_{net}$ ,  $LW_u$ , and  $LW_d$ . The statistics span 2000-2015.



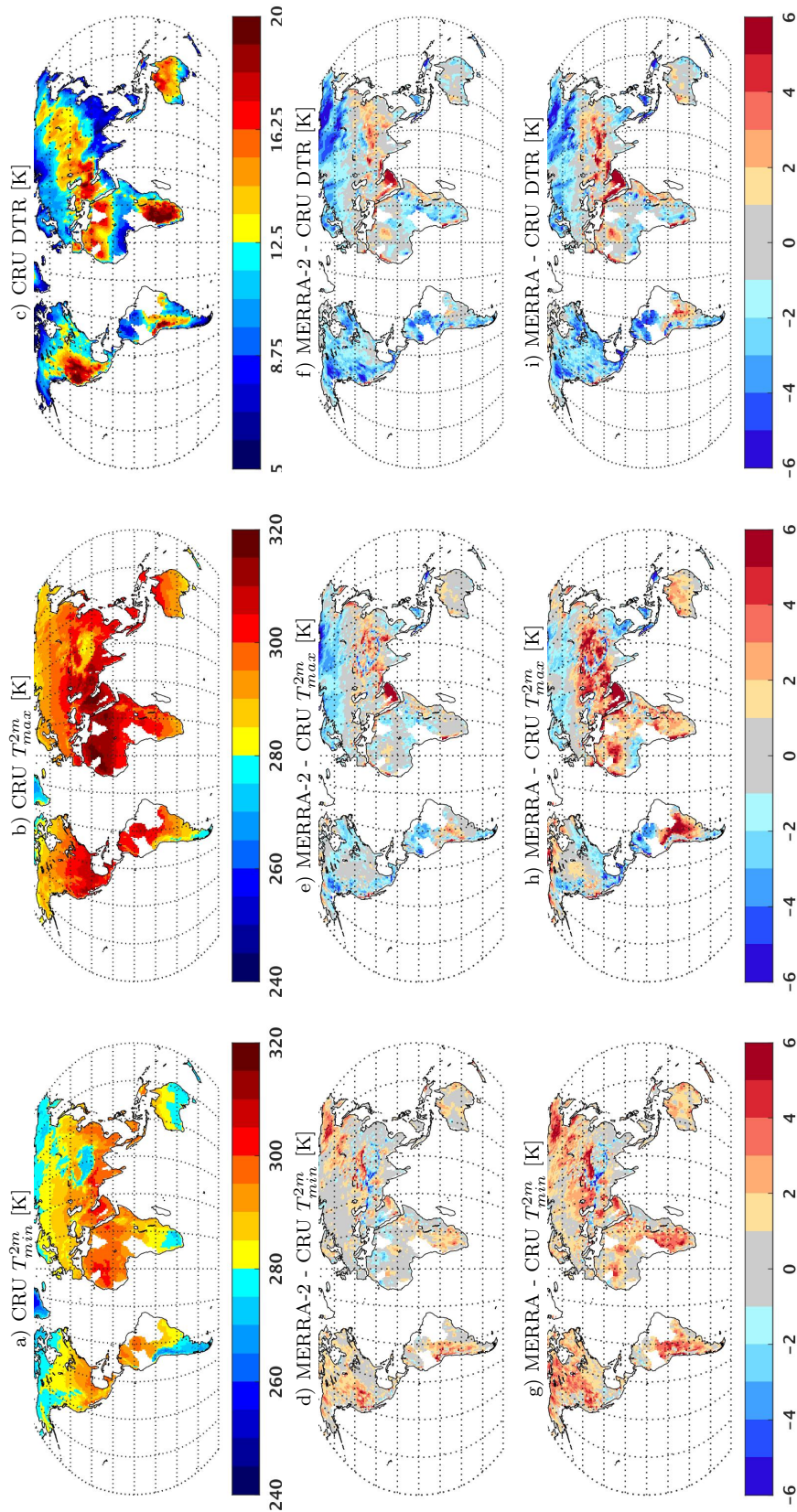


FIG. 7. The mean JJA  $T_{min}^{2m}$ , from CRU reference data (row 1), and the difference from the reference data for MERRA and MERRA-2 (rows 2-3), for the  $T_{min}^{2m}$  (column 1),  $T_{max}^{2m}$  (column 2), and the DTR (column 3). The statistics span 1980-2015, and white plotted over land indicates insufficient CRU data.

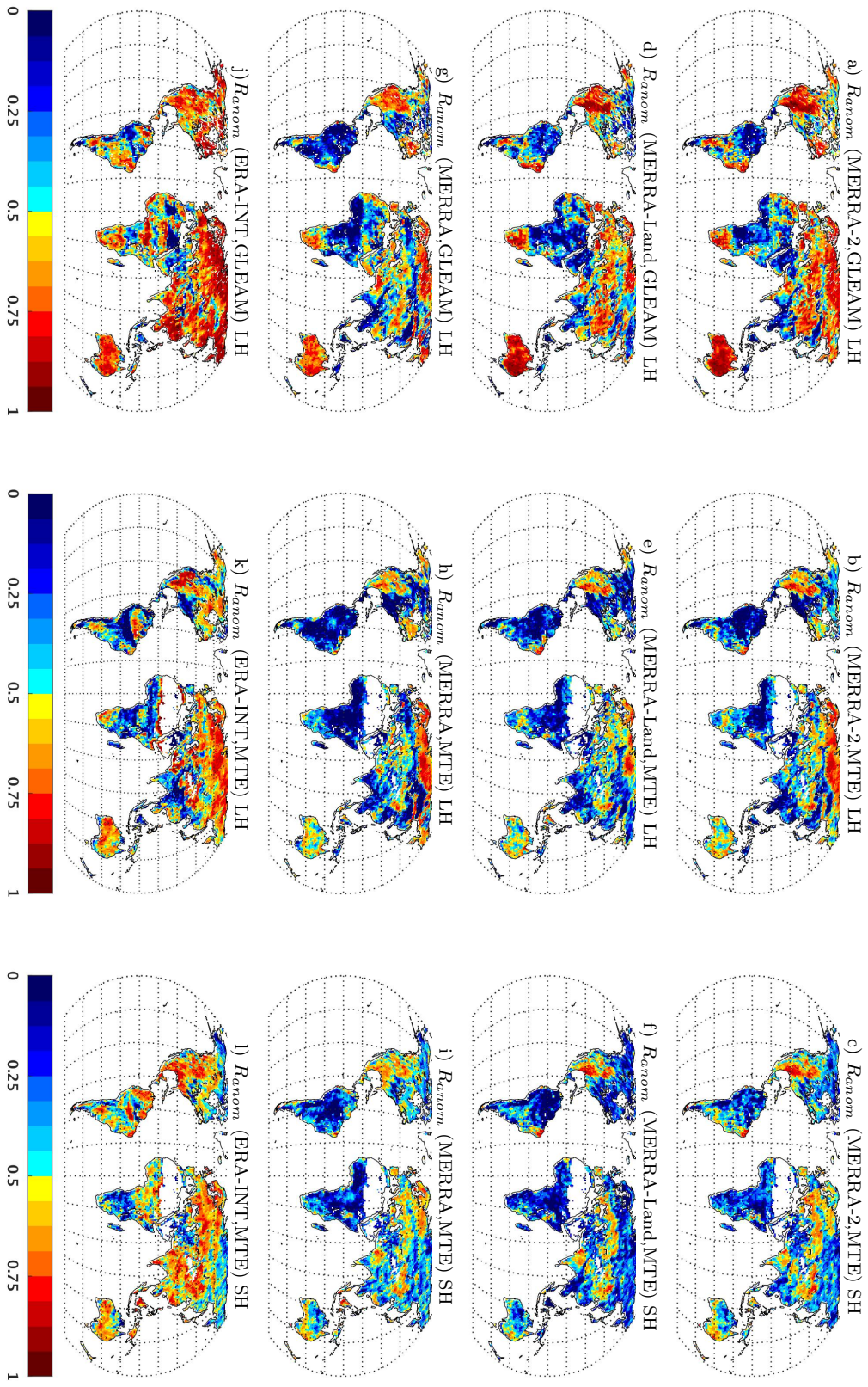


FIG. 8.  $R_{anom}$  between GLEAM LH, MTE LH, and MTE SH (columns 1-3) for MERRA, MERRA-Land, MERRA-2, and ERA-Interim (rows 1-4), for JJA. Statistics span 1980-2016 for GLEAM and 1982-2011 for MTE.

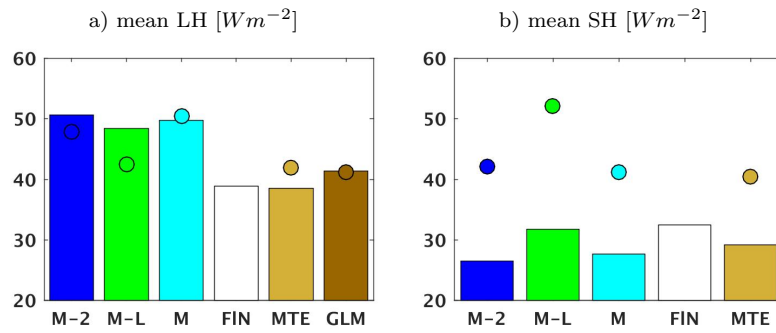


FIG. 9. Bar plot of the mean annual (a) LH and (b) SH, across the 20 Fluxnet site locations, from MERRA-2 (M-2), MERRA-Land (M-L), MERRA (M), Fluxnet (FIN), MTE, and GLEAM (GLM; LH only), calculated using each data set at its native resolution (and screened temporally for Fluxnet availability). For the global data sets, circles are plotted for the global land annual mean (taken from Figure 1).

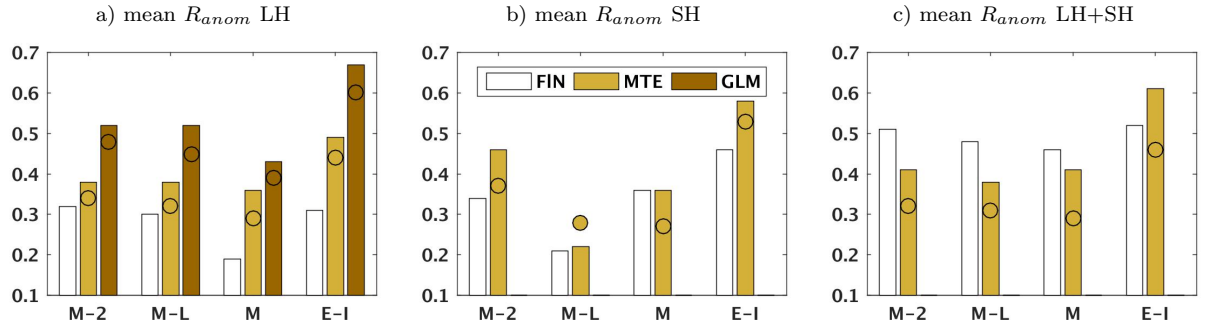


FIG. 10. Bar plot of the  $R_{anom}$  over JJA averaged across the 20 Fluxnet site locations, for (a) LH, (b) SH, and (c) LH+SH, between each pair of the reanalyses (MERRA-2 (M-2), MERRA-Land (M-L), MERRA (M), and ERA-I (E-I)) and the reference data (Fluxnet (FIN), MTE, and GLEAM (GLM)). The  $R_{anom}$  vs. the Fluxnet reference data use the reanalysis output at their reported spatial resolution (and screened temporally for Fluxnet availability), while the  $R_{anom}$  vs. GLEAM and MTE use reanalyses and reference data regridded to  $1^\circ$ . For GLEAM and MTE, circles are plotted for the global mean JJA  $R_{anom}$  (averaged over subplots of Figure 8).

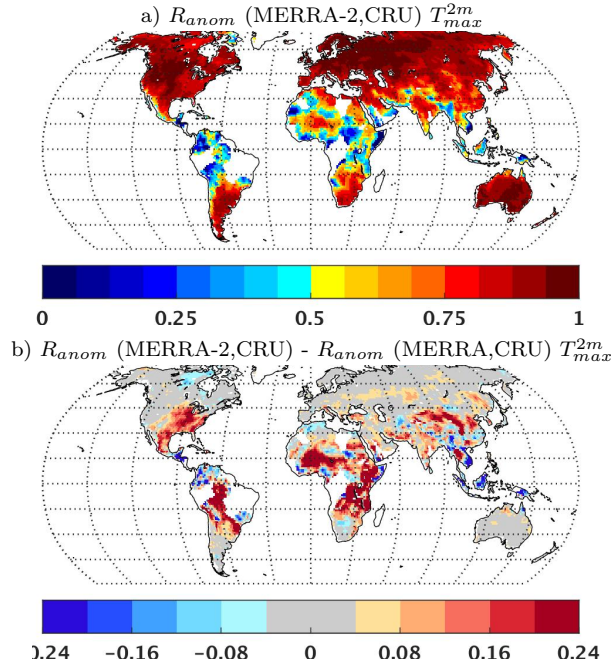


FIG. 11. The (a) MERRA-2  $R_{anom}$  vs. CRU monthly mean  $T_{max}^{2m}$ , and (b) the improvement in the  $T_{max}^{2m}$   $R_{anom}$  from MERRA to MERRA-2, both over JJA. Statistics span 1980-2015, and white plotted over land indicates insufficient CRU data.